XIV. STATISTICAL COMMUNICATION THEORY*

Prof. Y. W. Lee
Prof. A. G. Bose
Prof. D. J. Sakrison
Prof. M. Schetzen
Prof. H. L. Van Trees, Jr.
V. R. Algazi
R. Alter
D. S. Arnstein
M. E. Austin
R. F. Bauer
E. M. Bregstone
J. D. Bruce
A. M. Bush
J. K. Clemens
A. G. Gann
L. M. Goodman
C. E. Gray
T. G. Kincaid
A. J. Kramer
D. E. Nelsen
J. K. Omura
A. V. Oppenheim
R. B. Parente
J. S. Richters
W. S. Smith, Jr.
D. W. Steele

A. WORK COMPLETED

1. OPTIMUM SECOND-ORDER VOLTERRA SYSTEMS

This study has been completed by E. M. Bregstone. In May 1963, he submitted the results to the Department of Electrical Engineering, M. I. T., as a thesis in partial fulfillment of the requirements for the degree of Master of Science.

2. STUDY OF PHASE MODULATION WITH A GAUSSIAN SIGNAL

The present study has been completed by J. K. Clemens. It was submitted as a thesis in partial fulfillment of the requirements for the degree of Master of Science, Department of Electrical Engineering, M. I. T., May 1963.

M. Schetzen

3. MINIMIZATION OF ERROR PROBABILITY FOR A COAXIAL-CABLE PULSE-TRANSMISSION SYSTEM

This study has been completed by J. S. Richters. In May 1963, he submitted the results to the Department of Electrical Engineering, M. I. T., as a thesis in partial fulfillment of the requirements for the degree of Master of Science.

4. EXPERIMENTAL INVESTIGATION OF A SELF-OPTIMIZING FILTER

This study has been completed by W. S. Smith, Jr. He submitted the results to the Department of Naval Architecture, M. I. T., May 1963, as a thesis in partial fulfillment of the requirements for the degree of Master of Science and professional degree of Naval Engineer.

D. J. Sakrison

*This work was supported in part by the National Institutes of Health (Grant MH-04737-03); and in part by the National Science Foundation (Grant G-16526).

5. INFLUENCE OF NORMAL MODES OF A ROOM ON SOUND REPRODUCTION

This study has been completed by D. W. Steele. In May 1963, he submitted the results to the Department of Electrical Engineering, M. I. T., as a thesis in partial fulfillment of the requirements for the degree of Master of Science.

A. G. Bose

6. TRANSIENT BEHAVIOR OF A PSEUDO NOISE-TRACKING SYSTEM

This study has been completed by D. S. Arnstein. In May 1963, he submitted the results to the Department of Electrical Engineering, M. I. T., as a thesis in partial fulfillment of the requirements for the degree of Master of Science.

7. EXPERIMENTAL INVESTIGATION OF THRESHOLD BEHAVIOR IN PHASE-LOCKED LOOPS

This study has been completed by A. G. Gann and the results have been submitted to the Department of Electrical Engineering, M. I. T., May 1963, as a thesis in partial fulfillment of the requirements for the degree of Master of Science.

H. L. Van Trees, Jr.

B. A TWO-STATE MODULATION SYSTEM

A simple two-state modulation system was described in Quarterly Progress Reports No. 66 (pages 187-189) and No. 67 (pages 115-119). This report is a continuation of the analysis of this system and presents some of its applications.

1. Switching Frequency and Linearity

The block diagram of the modulation system is shown in Fig. XIV-1.

The general expressions for the time average $\overline{y}$ of the output y(t) and the switching period were given in Quarterly Progress Report No. 67 (page 116). Those expressions form the basis from which the dc performance of the system can be predicted. The nonlinearity of the system, defined below, is determined solely by the ratio of the zero-signal switching period to the time constant of the feedback network. Figure XIV-2 shows the percentage of nonlinearity as a function of the normalized output signal level with T_o/τ as the parameter. The percentage of nonlinearity is defined as

$$\frac{100 \cdot (\overline{y}-KE_s)}{\overline{y}}, \tag{1}$$

where K is the slope of $\overline{y}$ vs E_s as $E_s \to 0$. Notice that this definition of nonlinearity

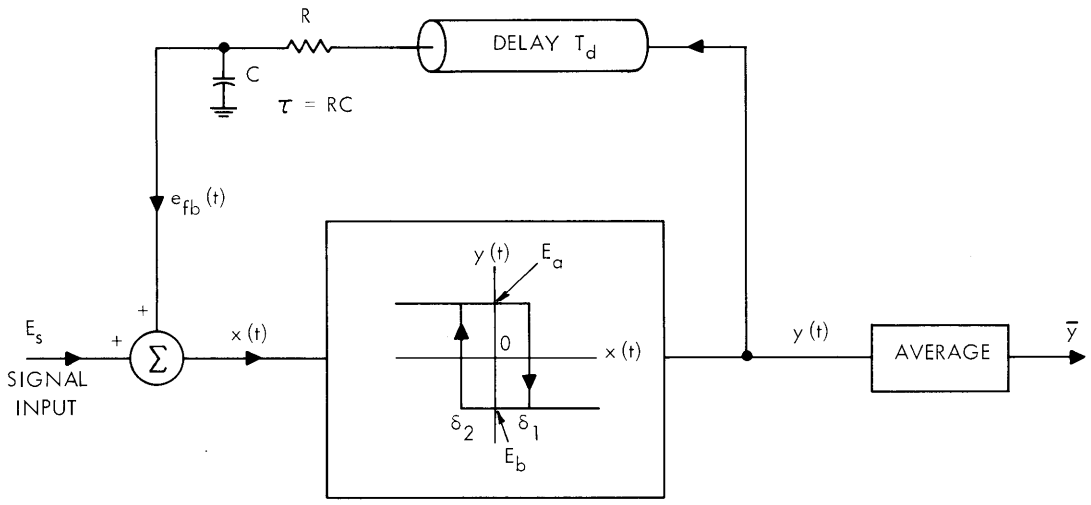

Fig. XIV-1. Modulation system with system parameters indicated.

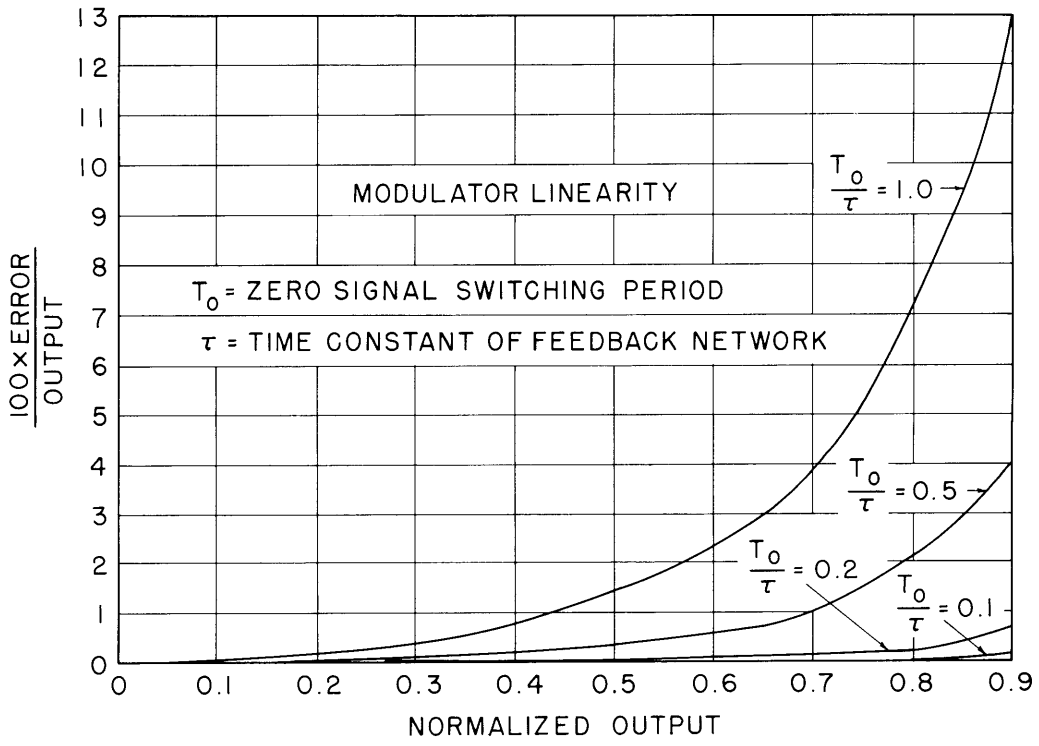

Fig. XIV-2. Modulator nonlinearity vs signal output.

is more stringent than the usual one in which the deviation is divided by the maximum output. The latter yields low distortion figures for systems that perform well with respect to large-amplitude signals but may badly distort small-amplitude signals.

For ac signals the time constant τ must be short enough so that the feedback network passes the highest signal frequency. If we arbitrarily set τ so that the half-power point of the feedback network occurs at twice the upper limit of the signal bandwidth B (cps), we have

$$T_o/\tau = 4\pi T_o B = 4\pi \frac{B}{f_o}, \tag{2}$$

where $f_o = \frac{1}{T_o}$ is the zero-signal switching frequency. Thus, for a given signal bandwidth B, this system achieves linearity at the cost of bandwidth.

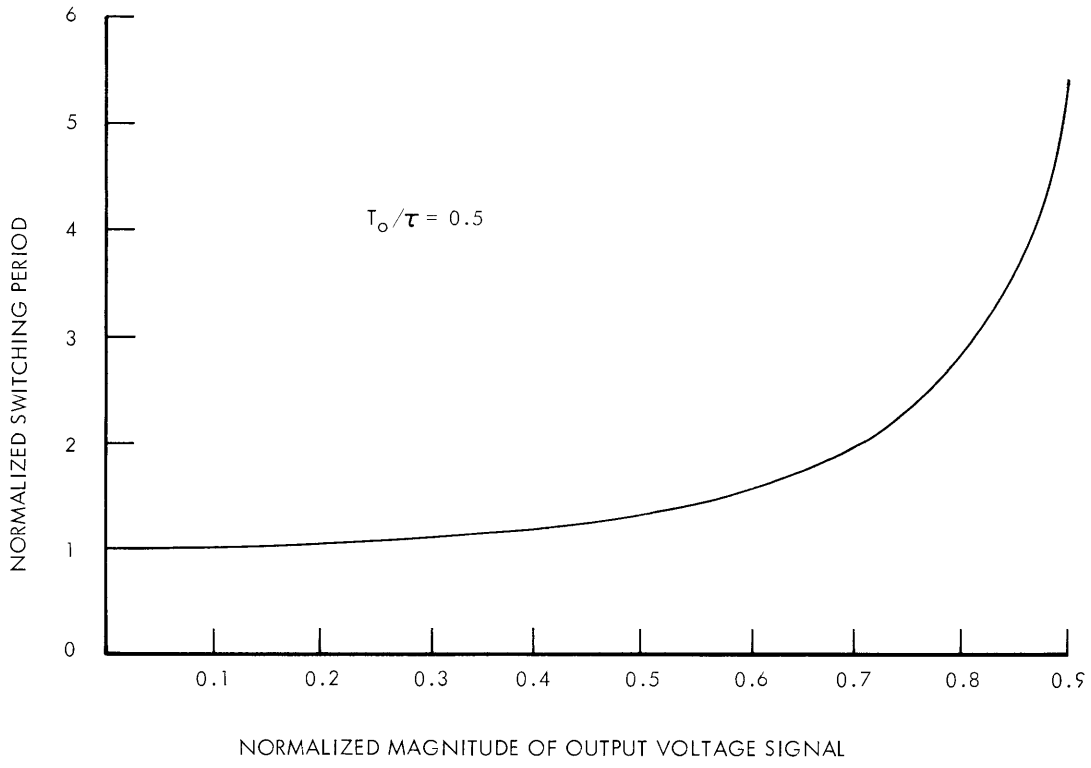

Fig. XIV-3. Switching period vs magnitude of output signal.

The switching frequency of the system increases monotonically with the magnitude of the output signal, as indicated in Fig. XIV-3, which shows the switching period as a function of the output-signal magnitude for dc signals. The curve is shown for $T_o/\tau = 0.5$.

2. The Modulator Used as a Regulator

The modulator can be used as a very simple regulator by taking advantage of the insensitivity of $\overline{y}$ to changes in the forward-loop saturation levels. Suppose that

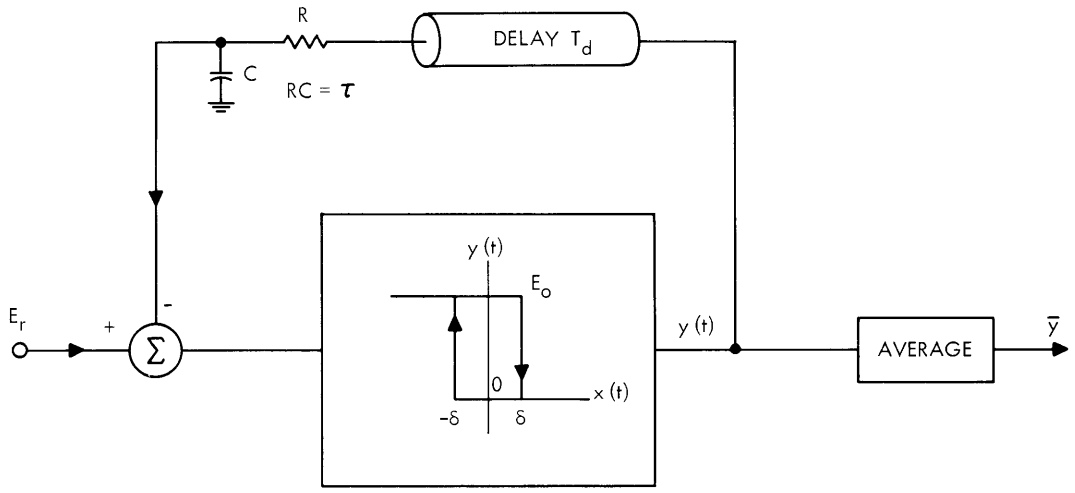

Fig. XIV-4. Regulator. Lower saturation level is set equal to zero to correspond to the voltage regulator example (see Fig. XIV-7).

we apply a dc reference signal E_r to the system shown in Fig. XIV-4. Analysis of this system for the output $\overline{y}$ yields the expression

$$\overline{y} = 1 - \frac{\ln\left(\dfrac{E_r - \delta}{E_o \exp(T_d/\tau) - E_o + E_r + \delta}\right)}{\ln\left(\dfrac{(E_r-\delta)(E_o-E_r+\delta)}{E_o \exp(T_d/\tau) - (E_o+E_r+\delta)(E_o \exp(T_d/\tau) - (E_r-\delta))}\right)}. \tag{3}$$

Preliminary calculations based on expression (3) and on measurements on an experimental model indicate that variations in the saturation level E_o can be suppressed more than 60 db at the output $\overline{y}$. They indicate that under all circumstances the regulation is improved by reducing the loop delay T_d. Curves showing the regulation as a function of the system parameters are being prepared.

3. Application to Nonlinear Control

The relay, or bang-bang servomechanism, is commonly used in control applications in which weight and power dissipation are significant considerations. The block diagram of such a controller is shown in Fig. XIV-5.

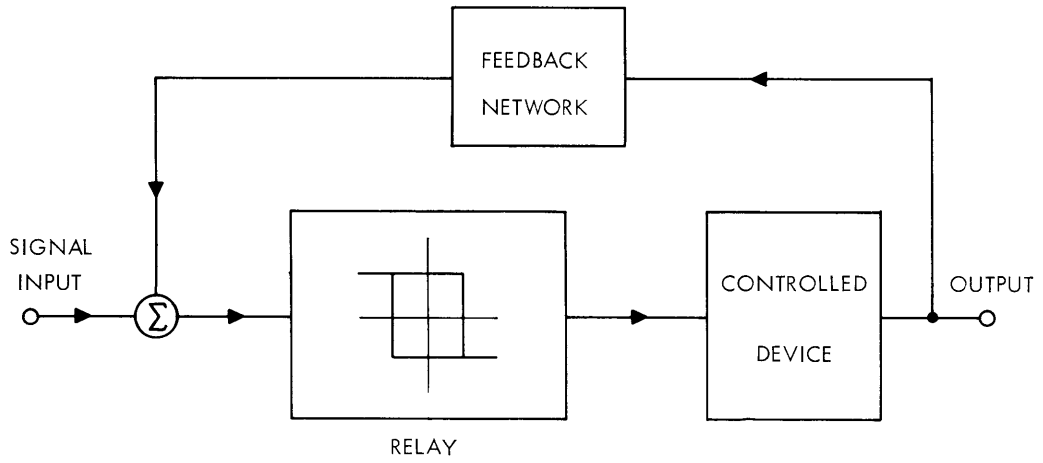

Fig. XIV-5. Simple relay servomechanism.

Briefly, the design of this system involves a compromise between static error, dynamic performance, and hunting. Hunting will always be present at the output unless the forward-loop nonlinearity contains a dead space. If a dead space is introduced, then sufficient damping, with its associated power loss, must be used to trap the system in the dead space. The damping requirement can be decreased by increasing the dead-space interval, but this is done by sacrificing the static error. These compromises are necessary because the system output (the output of the controlled device) is used to initiate the switching instants. Therefore switching must exist inherently at rates to which the controlled system responds.

By using the properties of the two-state modulator, it is possible to design a

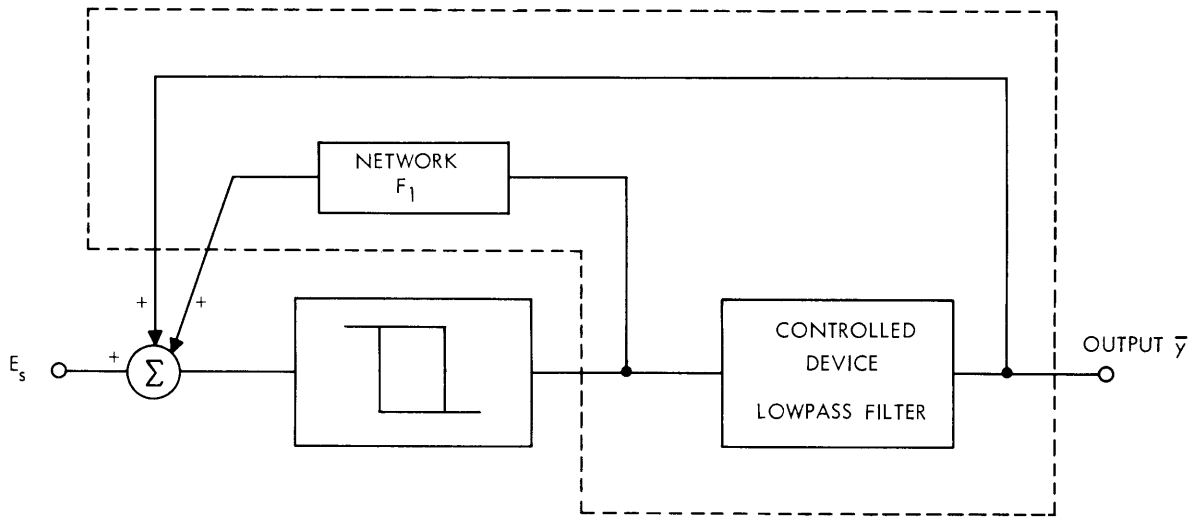

Fig. XIV-6. Nonlinear control system incorporating the modulator principle.

nonlinear controller that retains the advantages of low power dissipation, light weight, and, to a certain extent, the minimal settling time property, but eliminates the need for the dead space and damping usually employed to reduce hunting.

The block diagram of this controller is shown in Fig. XIV-6. The system within the dotted box comprises the total feedback network around the nonlinear forward loop. This network is divided into two paths. The result is that the network F_1 initiates an oscillation in the system at a frequency well beyond the response of the controlled device, and the over-all system still behaves linearly and has control with respect to load changes. The advantages of the low power dissipation of the relay servomechanism are preserved in the present system as long as the input to the controlled device is designed, as it can very easily be, to absorb no power at the high switching frequencies. In this design the ratio of the zero-signal switching frequency to the cutoff frequency of the controlled device can be made arbitrarily large without using active elements in the feedback loop and without introducing instability with respect to the system output. An analysis and the properties of this system will be presented in other reports. The application of the system to the problem of voltage control will be discussed here.

4. Voltage-Regulator Example

As an example of the nonlinear control discussed above, a simple voltage regulator was constructed (Fig. XIV-7). In this circuit the three transistors represent the nonlinear forward loop in Fig. XIV-6, L_ℓ and C_ℓ represent the controlled device, and R_1, R_2, C_1, C_2 represent the network F_1. This circuit was designed to supply 1 amp at

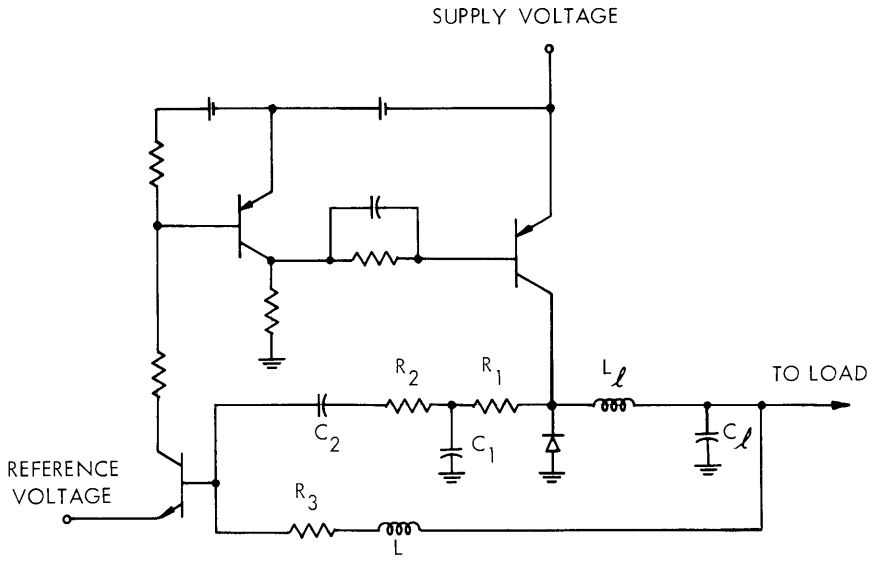

Fig. XIV-7. Voltage regulator that exemplifies nonlinear control.

15 volts to the load. The switching frequency was 100 kc. Measurements indicated better than 60-db attenuation of supply voltage variations at the load, and a change of only 0.14 per cent in the load voltage with a change by a factor of two in the load current.

5. D-C Transformer

Since each transistor in the realization of the modulator acts only as a switch, the system operates with high efficiency. From Eq. 3, it is possible to obtain any output voltage less than E - δ. Since the theoretical efficiency of the system is 100 per cent, we have the possibility of a very simple dc transformer, which works in the direction of stepping down voltages and stepping up currents, with the property that the power input equals the power output, and the additional feature that the output is regulated. Such a transformer was constructed by modifying the regulator of Fig. XIV-7 to obtain its reference voltage from its input as shown in Fig. XIV-8. This approach offers the possibility of building dc step-down transformers with efficiencies approaching those of conventional ac transformers, with the other features of lighter weight, smaller size, regulation, and adjustable "turns ratio." Thus in certain applications, in airborne equipment, for instance, there may be advantages in distributing dc instead of ac power. With ac power it is necessary, in each piece of equipment, first, to use a transformer, then to rectify, filter, and regulate. All of these operations could be carried out by a

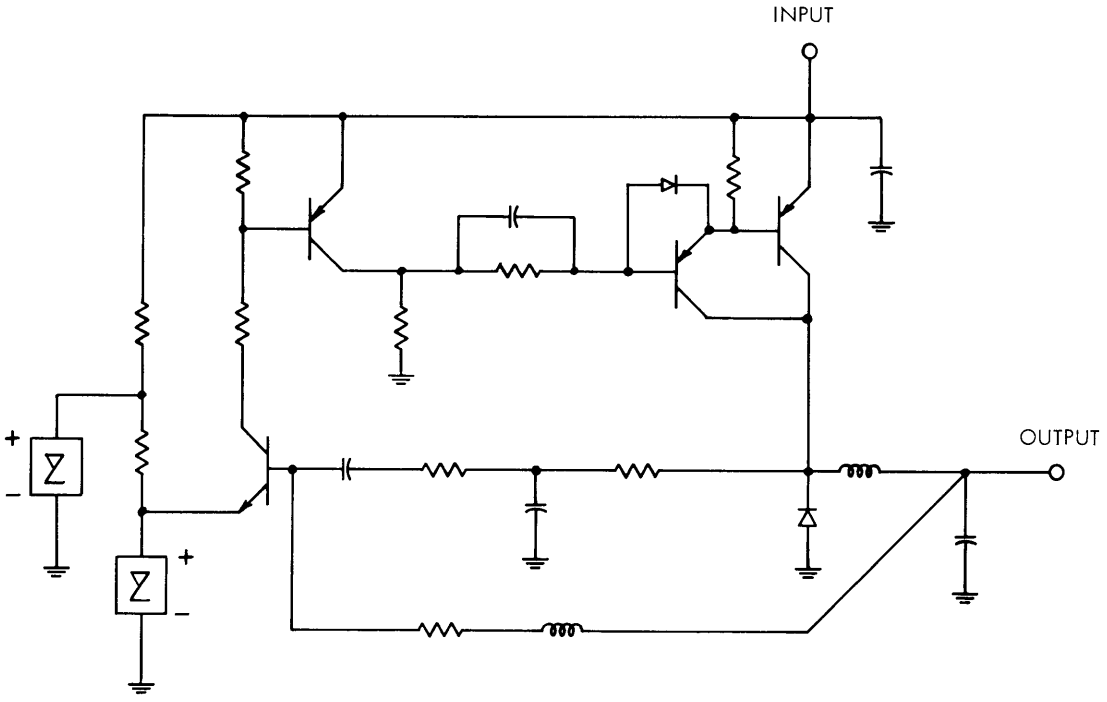

Fig. XIV-8. A dc transformer.

single dc transformer of the type discussed here. It should be noted, of course, that the dc transformer does not provide isolation and therefore would not suffice in an application for which it is essential. The transformer shown in Fig. XIV-8 was designed for only 15 watts power. However, it is possible, with existing transistors and similar circuitry, to construct transformers that deliver hundreds of watts.

6. Power Amplifier

The application of the modulation system to a dc-to-15-kc power amplifier is shown in Fig. XIV-9. The amplifier is designed to deliver 15 watts peak

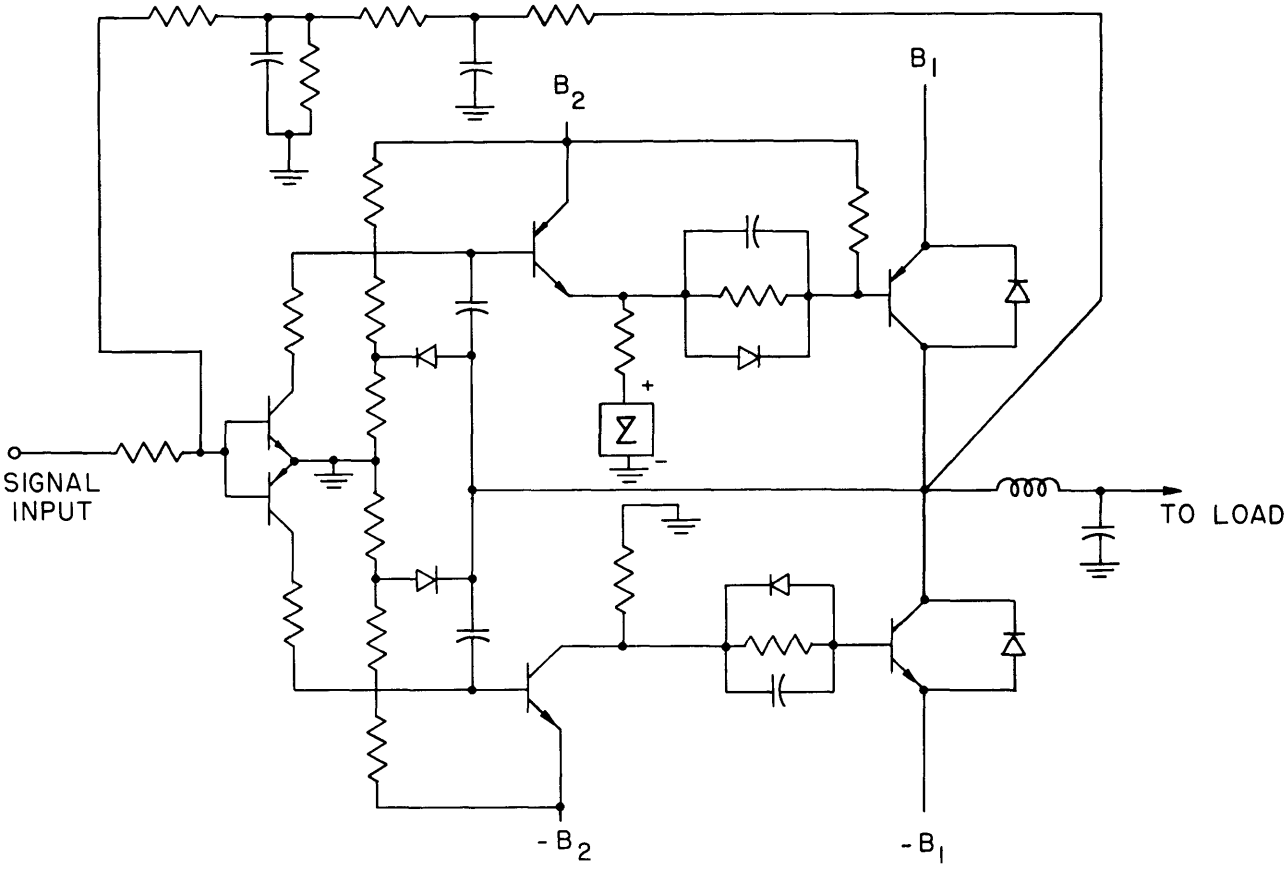

Fig. XIV-9. Circuit of 15-watt power amplifier.

power to a 16 Ω load. The mode structure and performance characteristics of this amplifier will be discussed in future reports.

A. G. Bose

C. OPTIMUM QUANTIZATION OF A SIGNAL CONTAMINATED BY NOISE

1. Formulation of the Problem

In a previous report[1] the problem of designing the optimum quantizer for a specific input signal was considered. An algorithm was developed by which the parameters defining the optimum quantizer can be calculated. The result is valid for a wide class of error criteria.

In many cases of interest, however, the signal is contaminated by noise before reaching the input of the quantizer. The noise may or may not be statistically independent of the signal. Mathematically, the quantizer input x may be written

$$x = s \oplus n, \tag{1}$$

where s is the signal, n is the noise, and $\oplus$ is a symbol that indicates some combination of the two variables, s and n. Two combinations of interest in communications

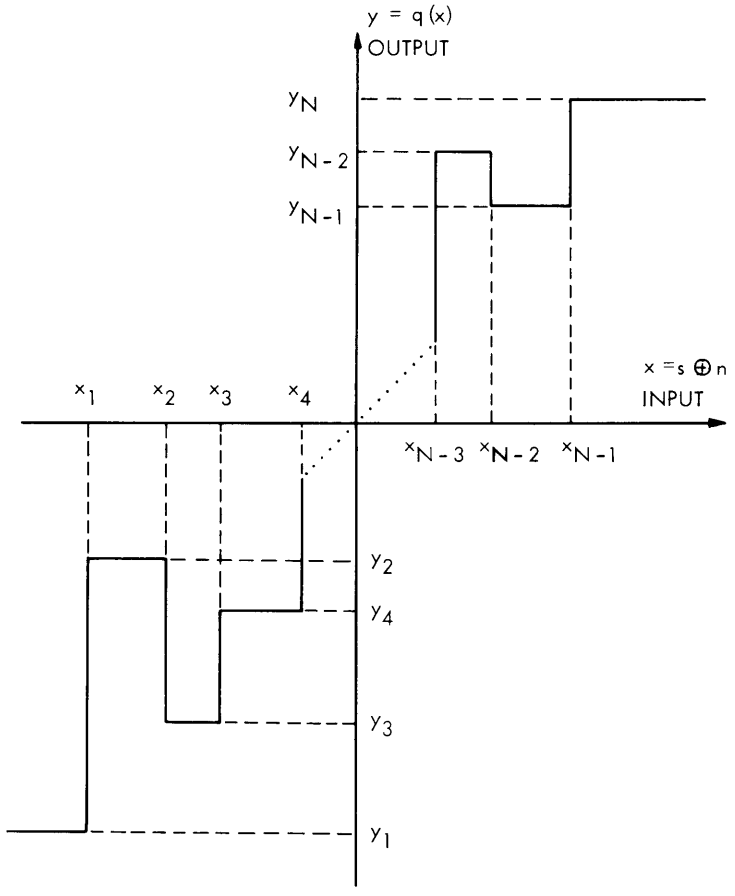

Fig. XIV-10. Input-Output relationship for a quantizer.

are (s+n) and (s·n). It will be seen from examination of Eq. 4 that any combination for which a joint probability density of x and s can be defined is an allowable combination.

The nonlinear, no-memory input-output characteristic of the quantizer, Fig. XIV-10, will be denoted by

$$y = q(x).$$

Then from (1) we have

$$y = q[s \oplus n]. \tag{2}$$

We desire to design a quantizer[2] that is such that its output y corresponds as closely as possible, with respect to some error criterion, to the signal s that is the desired quantizer output. Therefore, we shall take

$$s - q[s \oplus n] \tag{3}$$

to be the quantization error. The measure of the quantization error, that is, the quantity that we desire to minimize in order to minimize the quantization error, is taken to be the expected value of some function of the error $g[s-q(s\oplus n)]$, or equivalently, $g[s-q(x)]$. Then the measure of the error can be written

$$\mathscr{E} = \int_{-\infty}^{\infty} d\xi \int_{-\infty}^{\infty} d\eta \{g[\eta-q(\xi)]\, p_{x,s}(\xi,\eta)\}. \tag{4}$$

In Eq. 4, $p_{x,s}(\xi,\eta)$ is the joint probability density of the quantizer input x and the signal s.

Equation 4 can be simplified by considering the nature of the input-output characteristic of the quantizer. The output of the quantizer can take on only a fixed set of values; that is,

$$q(x) = y_i \qquad x_{i-1} \leq x < x_i, \quad i = 1, 2, \ldots, N \tag{5}$$

where x_o is defined as X_ℓ, the lower bound of the input signal x. Likewise, x_N is the upper bound of x, X_u. (These bounds are not required to be finite.)

Substituting (5) in (4), we obtain the following equation for the "error" in terms of the quantizer representation values:

$$\mathscr{E} = \sum_{i=0}^{N-1} \int_{U_i} d\xi \int_{V_i} d\eta \{g(\eta-y_{i+1})\, p_{x,s}(\xi,\eta)\}. \tag{6}$$

U_i is that set of values of ξ for which the output assumes the value y_{i+1}. From Eq. 5 we see that U_i depends only on the quantizer characteristic and corresponds to the set of values of ξ which are such that $x_i \leq \xi < x_{i+1}$. Thus, Eq. 6 can be written

$$\mathscr{E} = \sum_{i=0}^{N-1} \int_{x_i}^{x_{i+1}} d\xi \int_{V_i} d\eta \{g(\eta - y_{i+1})\, p_{x,s}(\xi,\eta)\}. \tag{7}$$

Analogously, V_i is the set of values of η over which the output assumes the value y_{i+1}. Referring to U_i, we see that V_i is equivalently that set of values of η which are such that when the signal and the noise are combined they yield a quantizer input in the range $x_i \leq \xi < x_{i+1}$. From Eq. 1 we see that V_i will depend upon the nature (or form) of the combination and upon the upper and lower bounds of the noise. Therefore, V_i cannot be explicitly expressed until the combination and the noise bounds are known. For purposes of formulating the method of determining the quantizer parameters, we shall utilize the "error" as given in Eq. 7.

Before we proceed with the task of determining the parameters of the optimum quantizer, let us demonstrate the method for determining the V_i. We shall consider two examples, assuming in each that Eq. 1 takes the specific form

$$x = s + n. \tag{8}$$

First, let us consider the case in which the noise is unbounded. Referring to Eq. 8, it is clear that any value of the signal can be transformed into the quantizer input region $x_i \leq \xi < x_{i+1}$ and therefore can be represented at the output by y_{i+1}. Thus, the set V_i is $-\infty \leq \eta < +\infty$. Then for this particular case, (7) becomes

$$\mathscr{E} = \sum_{i=0}^{N-1} \int_{x_i}^{x_{i+1}} d\xi \int_{-\infty}^{\infty} d\eta \{g(\eta - y_{i+1})\, p_{x,s}(\xi,\eta)\}. \tag{9}$$

As a second example, consider the case in which the noise is bounded with lower bound n_ℓ and upper bound n_u, that is, $n_\ell < n < n_u$. From Eq. 8 we see that values of the signal which are greater than $x_i - n_u$ can yield a quantizer input in the range $x_i < \xi$, since $n < n_u$. Also from (8) values of the signal which are less than $x_{i+1} - n_\ell$ can yield a quantizer input in the range $\xi < x_{i+1}$, since $n > n_\ell$. Thus, the set V_i which is the union of those values of the signal which correspond to $x_i < \xi$ and $\xi > x_{i+1}$ is expressed by the inequality

$$x_i - n_u < \eta < x_{i+1} - n_\ell.$$

Therefore, for this case (7) becomes

$$\mathscr{E} = \sum_{i=0}^{N-1} \int_{x_i}^{x_{i+1}} d\xi \int_{x_i - n_u}^{x_{i+1} - n_\ell} d\eta \{g(\eta - y_{i+1})\, p_{x,s}(\xi,\eta)\}. \tag{10}$$

2. Determination of the Optimum Quantizer

Equation 7 is an expression for the quantization error for an N-level quantizer. The optimum quantizer will be specified by specific values of x_i and y_k called X_i and Y_k, respectively. The X_i and Y_k specify the absolute minimum of (7) subject to the constraints

$$x_o < x_1 < x_2 \cdots < x_{N-1} < x_N. \tag{11}$$

These constraints are imposed only for organizational purposes.

At first, it might seem that the methods of calculus can be used to determine the X_i and Y_k. However, examination of the critical points of the error surface do not permit us to conclude that a critical point that is a relative minimum is also the absolute minimum within the region of variation specified by (11). Thus, in order to determine the X_i and Y_k we must turn to a more powerful technique, say, one that searches for the absolute minimum of the surface within the region of variation. Bellman's technique of dynamic programming[3,4] is such a technique.

In order to apply this technique, it is necessary to define three sets of functionals: the error functionals, $\{f_i(x_i)\}$; the transition-value decision functionals, $\{X_i(x)\}$; and the representation-value decision functionals, $\{Y_i(x)\}$. Each set of functionals has members for $i = 1, 2, \ldots, N$. These three sets of functionals are defined in the following manner:

$$\left.\begin{aligned}
f_1(x_1) &= \min_{\substack{y_1 \\ X_\ell = x_o \le x_1 \le X_u}} \left\{ \int_{x_o}^{x_1} d\xi \int_{V_o} d\eta \, [g(\eta - y_1)\, p_{x,s}(\xi,\eta)] \right\} \\
f_2(x_2) &= \min_{\substack{x_1, y_2 \\ X_\ell \le x_1 \le x_2 \le X_u}} \left\{ f_1(x_1) + \int_{x_1}^{x_2} d\xi \int_{V_1} d\eta \, [g(\eta - y_2)\, p_{x,s}(\xi,\eta)] \right\} \\
&\vdots \\
f_i(x_i) &= \min_{\substack{x_{i-1}, y_i \\ X_\ell \le x_{i-1} \le x_i \le X_u}} \left\{ f_{i-1}(x_{i-1}) + \int_{x_{i-1}}^{x_i} d\xi \int_{V_{i-1}} d\eta \, [g(\eta - y_i)\, p_{x,s}(\xi,\eta)] \right\} \\
&\vdots \\
f_N(x_N) &= \min_{\substack{x_{N-1}, y_N \\ X_\ell \le x_{N-1} \le x_N \le X_u}} \left\{ f_{N-1}(x_{N-1}) + \int_{x_{N-1}}^{x_N} d\xi \int_{V_{N-1}} d\eta \, [g(\eta - y_N)\, p_{x,s}(\xi,\eta)] \right\}
\end{aligned}\right\} \tag{12}$$

$$\left.\begin{aligned} X_1(x) &= X_\ell, \text{ a constant;} \\ X_2(x) &= \text{the value of } x_1 \text{ which corresponds to that in the definition of the functional } f_2(x_2),\ x_2 = x; \\ &\vdots \\ X_N(x) &= \text{the value of } x_{N-1} \text{ which corresponds to that in the definition of the functional } f_N(x_N),\ x_N = x \end{aligned}\right\}. \tag{13}$$

$$\left.\begin{aligned} Y_1(x) &= \text{the value of } y_1 \text{ which corresponds to that in the definition of the functional } f_1(x_1),\ x_1 = x; \\ Y_2(x) &= \text{the value of } y_2 \text{ which corresponds to that in the definition of the functional } f_2(x_2),\ x_2 = x; \\ &\vdots \\ Y_N(x) &= \text{the value of } y_N \text{ which corresponds to that in the definition of the functional } f_N(x_N),\ x_N = x \end{aligned}\right\}. \tag{14}$$

Consider these three sets of functionals for a few moments. The key to understanding them is understanding the meaning of the separate members of the error functionals (12). The first member of (12) states that for a given region of $p_{x,s}(\xi,\eta)$ specified by the boundaries x_o and x_1 (recall that V_o is specified in terms of x_o and x_1, and the nature of the noise contamination), we determine the y_1 that minimizes the integral

$$\int_{x_o}^{x_1} d\xi \int_{V_o} d\eta \left[g(\eta - y_1)\, p_{x,s}(\xi,\eta)\right]. \tag{15}$$

This y_1 is recorded as $Y_1(x)$, $x = x_1$ and the value of the integral (15) for this value of y_1 is recorded as $f_1(x_1)$. Thus, if we say that the region defined by the boundaries x_o and x_1 is to be quantized, we know that the optimum representation value for this interval is $Y_1(x_1)$.

Now consider the second functional of (12). This functional states that we are considering the quantization of the signal in the input interval $x_o \leq x \leq x_2$, for a variable x_2, into two levels. In order to perform this operation in the optimum manner, we must minimize the quantity

$$\int_{x_o}^{x_1} d\xi \int_{V_o} d\eta \, [g(\eta - y_1)\, p_{x,s}(\xi,\eta)] + \int_{x_1}^{x_2} d\xi \int_{V_1} d\eta \, [g(\eta - y_2)\, p_{x,s}(\xi,\eta)] \tag{16}$$

with respect to x_1, y_1, and y_2. However, the first of these two integrals when minimized with respect to y_1 (and it alone contains y_1) is simply the first error functional, $f_1(x_1)$. Then, for a specific x_2, we must determine the x_1 and the y_2 that minimize the function

$$f_1(x_1) + \int_{x_1}^{x_2} d\xi \int_{V_1} d\eta \, [g(\eta - y_2)\, p_{x,s}(\xi,\eta)]. \tag{17}$$

The x_1 that minimizes (17) is recorded as $X_2(x)$, $x = x_2$; the y_2 that minimizes the expression is recorded as $Y_2(x)$, $x = x_2$. The value of the expression is recorded as $f_2(x_2)$. Therefore, if the region $x_o \leq x < x_2$ is to be quantized into two levels, we know from the decision functionals that the optimum transition value is specified by $X_1 = X_2(x_2)$ and that the two optimum representation values are given by $Y_2 = Y_2(x_2)$ and $Y_1 = Y_1(x_1)$.

Clearly, discussion of this type can be presented for each of the members of (12). However, instead of considering every member, let us skip to the last functional in (12). Here, we are given the input range $x_o \leq x < x_N$; a variable x_N is assumed. We want to quantize this range into N levels in the optimum manner. This requires that we minimize the quantity

$$\int_{x_o}^{x_1} d\xi \int_{V_o} d\eta \, [g(\eta - y_1)\, p_{x,s}(\xi,\eta)] + \int_{x_1}^{x_2} d\xi \int_{V_1} d\eta \, [g(\eta - y_2)\, p_{x,s}(\xi,\eta)]$$

$$+ \ldots + \int_{x_{N-1}}^{x_N} d\xi \int_{V_{N-1}} d\eta \, [g(\eta - y_N)\, p_{x,s}(\xi,\eta)] \tag{18}$$

with respect to the parameters $y_1, y_2, \ldots, y_N; x_1, x_2, \ldots, x_{N-1}$. This task is not as difficult as it may seem. Note that the minimum of the first term with respect to y_1 as a function of x_1 is given by $f_1(x_1)$. This is the only term of (18) involving y_1. Thus (18) can be written alternately as the minimization of

$$f_1(x_1) + \int_{x_1}^{x_2} d\xi \int_{V_1} d\eta \, [g(\eta - y_2)\, p_{x,s}(\xi,\eta)] + \int_{x_2}^{x_3} d\xi \int_{V_2} d\eta \, [g(\eta - y_3)\, p_{x,s}(\xi,\eta)]$$

$$+ \ldots + \int_{x_{N-1}}^{x_N} d\xi \int_{V_{N-1}} d\eta \, [g(\eta - y_N)\, p_{x,s}(\xi,\eta)] \tag{19}$$

with respect to $y_2, y_3, \ldots, y_N; x_1, x_2, \ldots, x_{N-1}$. But the minimization of the first two terms of (19) with respect to y_2 and x_1 as a function of x_2 is given by $f_2(x_2)$. Again, these are the only terms involving y_2 and x_1. Thus we can again reduce the complexity of the expression to be minimized. Equation 19 can be equivalently written as the minimization of

$$f_2(x_2) + \int_{x_2}^{x_3} d\xi \int_{V_2} d\eta \, [g(\eta - y_2)\, p_{x,s}(\xi,\eta)] + \int_{x_3}^{x_4} d\xi \int_{V_3} d\eta \, [g(\eta - y_3)\, p_{x,s}(\xi,\eta)]$$

$$+ \ldots + \int_{x_{N-1}}^{x_N} d\xi \int_{V_{N-1}} d\eta \, [g(\eta - y_N)\, p_{x,s}(\xi,\eta)] \tag{20}$$

with respect to $y_3, y_4, \ldots, y_N; x_2, x_3, \ldots, x_{N-1}$.

This process is easily continued until we obtain as an equivalent for (20) the minimization of

$$f_{N-1}(x_{N-1}) + \int_{x_{N-1}}^{x_N} d\xi \int_{V_{N-1}} d\eta \, [g(\eta - y_N)\, p_{x,s}(\xi,\eta)] \tag{21}$$

with respect to x_{N-1} and y_N. For a specific x_N, the x_{N-1} and y_N that minimize (21) are recorded as $X_N(x)$ and $Y_N(x)$, respectively, $x = x_N$. The value of (21) for a specific x_N is recorded as $f_N(x_N)$.

Observe, now, that when $x_N = X_u$, we are considering the entire input signal range. Thus, $f_N(X_u)$ is the total quantization error for the optimum N-level quantizer. Then from the definition of $X_N(x)$, the $(N-1)^{th}$ transition value is

$$X_{N-1} = X_N(X_u).$$

Likewise, from the definition of $Y_N(x)$ the $(N)^{th}$ representation value is

$$Y_N = Y_N(X_u).$$

Continuing from our definition of $X_{N-2}(x)$ and $Y_{N-2}(x)$, we find that the next transition value is

$$X_{N-2} = X_{N-1}(X_{N-1})$$

and the next representation value is

$$Y_{N-1} = Y_{N-1}(X_{N-1}).$$

This process can clearly be continued until finally we have

$$Y_1 = Y_1(X_1),$$

which is the last parameter needed to completely define the optimum quantizer.

At present, our research is concentrated on the properties of the error surface. It is hoped that a knowledge of the error surface properties will simplify the determination of the parameters defining the optimum quantizer.

J. D. Bruce

References

1. J. D. Bruce, Optimum quantization for a general error criterion, Quarterly Progress Report No. 69, Research Laboratory of Electronics, M. I. T., April 15, 1963, pp. 135-141.

2. L. I. Bluestein, A Hierarchy of Quantizers, Ph. D. Thesis, Columbia University, May 1962, has considered a similar problem. He has been able to obtain an exact solution in the case of a discrete signal but only an approximate solution in the case of a continuous signal. In each case his error criterion was mean-absolute.

3. R. Bellman and J. Dreyfus, Applied Dynamic Programming (Princeton University Press, Princeton, New Jersey, 1962).

4. R. Bellman and B. Kotkin, On the Approximation of Curves by Linear Segments Using Dynamic Programming – II, Memorandum RM-2978-PR, The Rand Corporation, Santa Monica, California, February 1962.

D. MINIMIZATION OF ERROR PROBABILITY FOR A COAXIAL-CABLE PULSE-TRANSMISSION SYSTEM

We shall consider a particular pulse code modulation system visualized as one repeater link in a high-speed data-transmission facility. This system is illustrated in Fig. XIV-11. The criterion used in evaluating system performance is the probability of error at the system output, calculated by considering as degradations thermal noise and intersymbol interference from pulses that are no more than four time slots away in both the past and future. The system input is assumed to be a pulse train $s_{i_k}(t-kT)$, $k = 1, 2, 3, \ldots$. Each signal $s_i(t)$ is zero everywhere except on an interval $0 \leq t \leq T$. This set of possible input pulses is assumed to be binary, and the two possible signals are assumed to have equal energies and to be a priori equiprobable. Successive pulses are assumed to be statistically independent.

The transmission medium was chosen to be a 22-gauge paper-insulated two-wire line, 6000 feet long. This is the same type of line actually used in an experimental system at Bell Telephone Laboratories.[1] Also, to obtain solutions to some of the problems considered, it is necessary to use a rational expression for H(s); thus an approximation of the form $H(s) = \frac{A\omega_1\omega_2}{(s+\omega_1)(s+\omega_2)}$ was assumed, with $A = 0.4$, $\omega_1 = 5.03 \times 10^5$, and

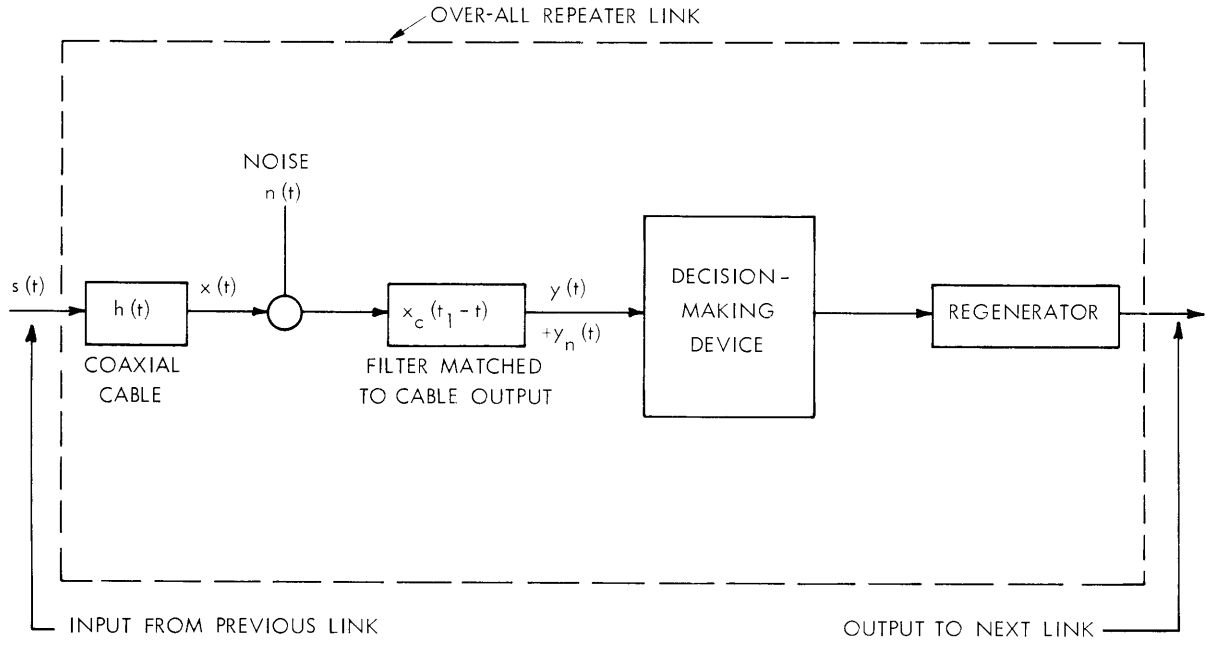

Fig. XIV-11. Block diagram of the system.

$\omega_2 = 5.03 \times 10^6$. This approximation was found to be "good" in both the time and frequency domains by Bell Telephone System engineers when the pulses were sent at a rate of 1.544 megabits per second. Therefore, the signal period T and the approximation to H(s) were used exactly as set forth by Mayo.[1]

At the cable output, additive noise, denoted n(t), was introduced. This is assumed to be white Gaussian thermal noise produced by the cable, with available noise power of kT/2 watts/cps (in a double-sided spectrum), where k is Boltzmann's constant, and T = 293°K = 68°F.[2] This thermal noise is assumed to be the only source of noise present.

The first stage of a repeater is usually some sort of filter to improve the signal-to-noise ratio going into the detector. In general, we are free to vary the shape of this filter at will, but, in order to cut down the number of variables involved in this problem, the filter was assumed to be matched to the cable output pulse x(t). In other words, the impulse response of the filter is $x_c(t_1-t)$, where

$$x_c(t) = \begin{cases} x(t) & 0 < t < t_1 \\ 0 & \text{elsewhere.} \end{cases}$$

We assume that t_1 is very large (in the sense that $x(t) \approx 0$ for $t \geq t_1$) and thus we may make the approximation $x_c(t_1-t) \approx x(t_1-t)$. Such a filter maximizes the signal-to-noise ratio at the output for any given x(t), and hence in the absence of interpulse interference

it minimizes the probability of error. This is not necessarily the best choice of filter, however, since other filters giving smaller output signal-to-noise ratios may give less intersymbol interference and thus smaller probability of error. The filter is followed by an instantaneous voltage sampler, a detector, and a regenerator.

Since the input signals are binary, equiprobable, and of equal energies, the signals will be of the form s(t) and -s(t) for a minimum error probability at the output.[3] The detector decision level should be set at zero, under the assumption that the two possible types of errors are equally harmful. For each problem considered, the optimization carried out was a variation of the input signal s(t) to determine the signal that resulted in the minimum error probability.

The first problem considered was to determine the input signal s(t) that maximizes the output signal-to-noise ratio (thereby minimizing error probability if only the noise is taken into account) for $\int_0^T s^2(t)\,dt$ constrained to be E. This problem is equivalent to that of maximizing the signal energy at the cable output with fixed input energy. Originally, the problem was considered to be the first step in a perturbation approach to our original problem, and its solution would minimize error probability when the effects of intersymbol interference are neglected. We hoped that this solution would not yield a prohibitive amount of intersymbol interference. This solution would then not differ by a great deal from the desired solution of the original problem, that of minimizing the probability of error. The desired solution then possibly could be obtained by perturbation techniques. This was not possible, since the solution of this problem resulted in an output pulse with such large amounts of interference that intersymbol interference from only two adjacent pulses was sufficient to cause an error in one of four cases.

The second problem was to determine the signal s(t) with fixed energy E which would maximize output signal-to-noise ratio, with the constraint that the amount of intersymbol interference one time slot away from the peak in either direction is a value K. Then the value of K was varied to obtain the minimum probability of error. By using simple variational procedures, an integral equation of the form

$$s(t) = \frac{1}{\lambda}\int_0^T s(u)\left[R_{hh}(t-u)+\mu(R_{hh}(t-u+T)+R_{hh}(t-u-T))\right]du \tag{1}$$

was derived. In Eq. 1, λ and μ are Lagrangian multipliers that must be determined, and $R_{hh}(t) = \int_0^\infty h(a)\,h(a+t)\,da$. This equation is not always soluble, but in the special case in which H(s) is a rational function of s, the integral equation can be transformed into a simple differential equation that is easily solved.[4] The differential equation was derived and solved. For the two-pole approximation to H(s), the solution is of the form

$$s(t) = c_1\left(e^{p_1 t} + c_2 e^{-p_1 t} + c_3 \cos p_2 t + c_4 \sin p_2 t\right) \tag{2}$$

for $0 \leq t \leq T$, and $s(t) = 0$ elsewhere. This is the general form of $s(t)$ for the maximization, and λ, μ, and the c_i were determined from the interference constraint, the fixed-input energy constraint, and the boundary conditions on the integral equation. These were determined numerically through use of the IBM 7090 digital computer at the Computation Center, M. I. T. Note that the first problem considered (no interference constraint) is a special case of this one, and follows from Eq. 1 if we set $\mu = 0$.

A third problem was that of constraining intersymbol interference to be zero at one and two time slots away from the pulse peak and again maximizing output signal-to-noise ratio. This constraint can be shown to constrain the interference to be zero for all time, since we have assumed that H(s) is a two-pole rational function of s. Thus this problem is equivalent to one investigated by Holsinger.[5] Solutions can be obtained by his methods, which are much simpler than the integral-equation method that one would otherwise use. For most values of input energy, the solutions of this problem resulted in lower values of error probability than those found by constraining intersymbol interference one time slot away and varying the constraint for minimum error probability. For low input energies, the previous solutions gave better results, but this might be due to the fact that error probabilities were calculated by assuming interactions from only four pulses away, while in reality pulses farther away have nonnegligible interference. This will, of course, not affect error probabilities calculated for the pulse with zero interference, but error probabilities calculated for other pulses will be somewhat lower than their true values.

The final results were that

(1) Maximizing signal-to-noise ratio without considering intersymbol interference produces a solution that is unusable in an error probability sense.

(2) Maximizing signal-to-noise ratio while constraining intersymbol interference one time slot away and then varying the constraint for minimum error probability produces usable solutions, but in most cases not as good as those for result (3).

(3) Maximizing signal-to-noise ratio while constraining intersymbol interference to be zero one and two time slots away, which, for the assumptions made about the cable transfer function, results in zero interference everywhere.

These results are given in greater detail in the author's thesis.[6]

J. S. Richters

References

1. J. S. Mayo, A bipolar repeater for pulse code signals, Bell System Tech. J. 41, 25-97 (1962).

2. A. Van der Zeil, Noise (Prentice-Hall, Inc., Englewood Cliffs, N. J., 1954).

3. G. L. Turin, An introduction to matched filters, Trans. IRE, Vol. IT-6, No. 3, pp. 311-329, June 1960.

4. W. B. Davenport and W. L. Root, Random Signals and Noise (McGraw-Hill Book Company, Inc., New York, 1958), pp. 371-382.

5. J. Holsinger, Some Problems Involved in Communication over a Class of Channels with Memory, Course 6.68 Special Problem Report, M. I. T., 1962.

6. J. S. Richters, Minimization of Error Probability for a Coaxial Cable Pulse Transmission System, S. M. Thesis, Department of Electrical Engineering, M. I. T., May 17, 1963.

E. EXPERIMENTAL INVESTIGATION OF A SELF-OPTIMIZING FILTER

1. Introduction

An experimental verification of the continuous adjustment procedure considered by Sakrison[1] is undertaken in this report. The adjustment procedure permits design of a filter system of the form shown in Fig. XIV-12 by the continuous adjustment of the k coefficients $x_1, x_2, \ldots, x_k$. The purpose of the adjustment procedure is to search out and converge to the coefficient setting that yields minimum average weighted error. The only assumption that we make on the weighting function is that it be convex. The adjustment procedure operates by estimating the gradient of the regression surface being searched and adjusting the values x_i, $i = 1, 2, \ldots, k$, to move the system error toward its minimum. Through the function c(t), a known plus and minus perturbation is introduced to the present setting of each of the x_i. When the errors resulting from these plus and minus perturbations of the i^{th} parameter are measured, weighted by the chosen error weighting function, and subtracted, the resultant function, $Y_i(t)/c(t)$, is a random variable whose mean is a difference approximation of the i^{th} component of the gradient in the direction of the optimum. The function a(t) is a monotonically decreasing function that is then used to weight the value of the gradient. The parameter change is then

$$x_i(t) = x_i(\phi) - \int_0^t \frac{a(\tau)}{c(\tau)} Y_i(\tau)\, d\tau.$$

It has been shown[1] for certain choices of the functions a(t) and c(t) and under our assumption of a convex error weighting function and under certain regularity assumptions on the processes, that the procedure will converge in the sense that

$$\lim_{t\to\infty} E\left\{(x_i(t)-\theta_1)^2\right\} = 0 \qquad i = 1, 2, \ldots k$$

in which θ_1 denotes the optimum setting for the coefficient x_i. The functions $a(t) = K_a/(at+b)^{oc}$ and $c(t) = K_c/(t+d)$ satisfy the conditions for convergence if

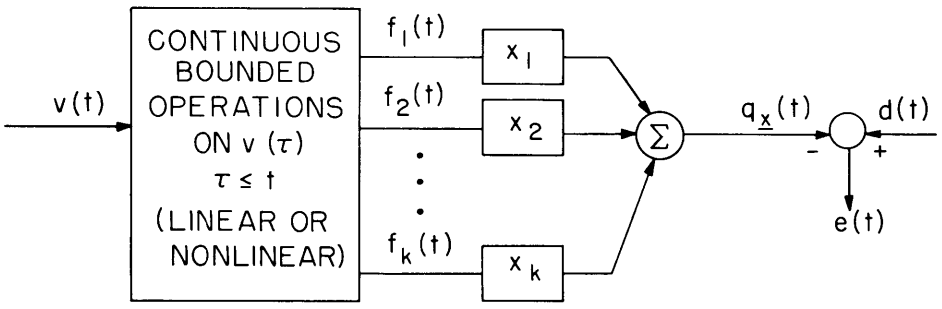

Fig. XIV-12. Form of the filter (or predictor or model) to be designed. (This is D. J. Sakrison's Fig. XIII-3, Quarterly Progress Report No. 66, p. 192.)

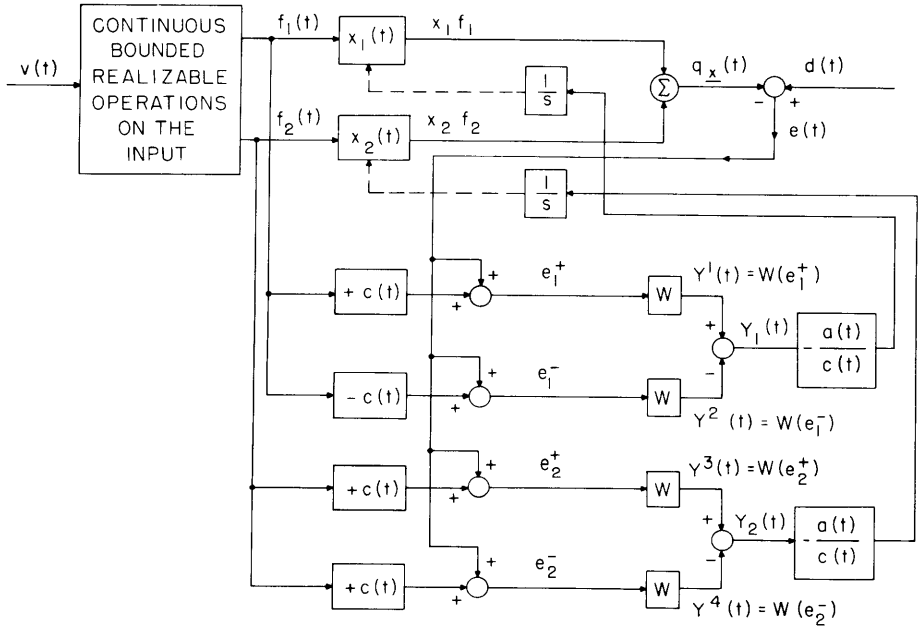

$$x_1(t) = x_1(1) - \int_1^t \frac{a(\tau)}{c(\tau)}\, Y_1(\tau)\, d\tau$$

$$x_2(t) = x_2(1) - \int_1^t \frac{a(\tau)}{c(\tau)}\, Y_2(\tau)\, d\tau$$

$$e_1^+ = -f_1(t)\left[x_1(t) + c(t)\right] - f_2(t)\, x_2(t) + d(t)$$

$$e_1^- = -f_1(t)\left[x(t) - c(t)\right] - f_2(t)\, x_2(t) + d(t)$$

$$e_2^+ = -f_1(t)\, x_1(t) - f_2(t)\left[x_2(t) + c_2(t)\right] + d(t)$$

$$e_2^- = -f_1(t)\, x_1(t) - f_2(t)\left[x_2(t) - c_2(t)\right] + d(t)$$

Fig. XIV-13. Diagram of the continuous adjustment procedure for two parameters, x_1 and x_2.
(This is D. J. Sakrison's Fig. XIII-4, Quarterly Progress Report No. 66, p. 192.)

$1/2 < o \cdot c \leq 1$ and $\delta > (1-o \cdot c)/4$.

2. A Self-Optimizing Filter

Fant[2] describes the long-term average of speech as being characterized by a 12-db octave decay over the audio spectrum. He also shows some curves of the actual spectrum which suggest that restricting the circuit usage to certain types of messages (that is, a tactical voice circuit) would result in a power density spectrum that would follow the 12-db curve on the average but would have significant plus and minus perturbations from this mean. Such a desired output spectrum is approximately a staircase function with steps of uneven height following the mean of 12 db per octave slope. Thus an investigation was made of a "self-optimizing" filter system for separating such an audio signal from broadband noise. This filter consisted of k third-order lowpass filters spaced linearly throughout the useful portion of the audio band (250 to 2500 cps contains most of the useful intelligibility). This system compares the desired output with that actually being received and adjusts the coefficients of the k filters for minimum mean-square error by the method just described. The mechanization of the adjustment procedure is shown in block diagram form in Fig. XIV-13. Although the desired output signal was used here in carrying out the adjustment procedure, it was done only for convenience: for the case considered here, the adjustment procedure could be carried out without the desired signal.[3]

3. Experimental Procedure

Experimental work was undertaken to ensure that the adjustment procedure would lead to system parameter convergence on available analog equipment. In particular, it was desired to know if the system parameters would converge within a time suitable for the application proposed and if the adjustment procedure is critically dependent on any of the adjustment parameters.

A filter system consisting of two lowpass filters combined with variable coefficients x_1 and x_2 was studied in detail for a mean-square error criterion. This criterion was chosen because it permitted an easy analytical check on the performance of the adjustment procedure. On completion of these studies, checks were made for a system of 4 lowpass filters to ensure that the adjustment procedure still led to the proper results.

The desired output, d(t), is obtained by passing the output of a white noise generator (having power density spectrum S_o) through a filter of the form

$$\frac{K}{(j\omega + 628)^2}.$$

This gives the desired approximation of a mean speech spectrum. The input was formed by adding to the desired output white noise from another generator having essentially a

a flat power density spectrum of magnitude N.

For the mean-square error criterion, the term $\frac{1}{c(\tau)} Y_i(\tau)$ is independent of $c(\tau)$ and we need only a(t). The function a(t) was generated by dividing a ramp of the form A't + 2 into $Y_1(t)$ and multiplying the output of this operation by integrator gain D so that the form of a(t) was D/(A't+2).

For purposes of this report, convergence time is defined as the time elapsed from activation of the system until the last time that the mean-square error (as found by time-averaging over a suitable interval) falls within 10 per cent of its minimum value. That region containing all those points having their mean-square error within 10 per cent of the minimum value is hereafter called the convergence area.

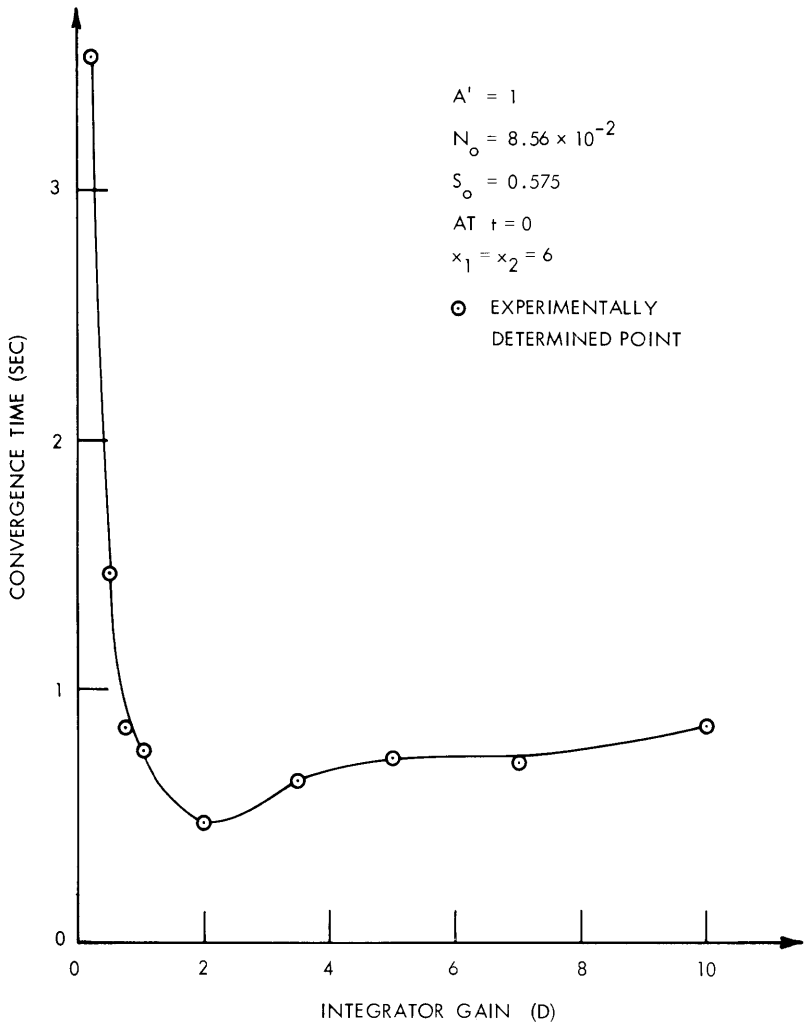

Fig. XIV-14. Convergence time versus integrator gain (D).

4. Results

Figure XIV-14 shows the convergence time versus the integrator gain, D. From this figure it is seen that large convergence time is obtained for integrator gains approaching zero. Settings between one and seven gave suitable convergence with initial oscillations about the convergence area, the amplitude of the oscillations increasing with increasing gains. Minimum convergence time was obtained for a setting of D just less than that value which first results in oscillations.

Figure XIV-15 shows the coefficient setting yielding minimum error, the convergence

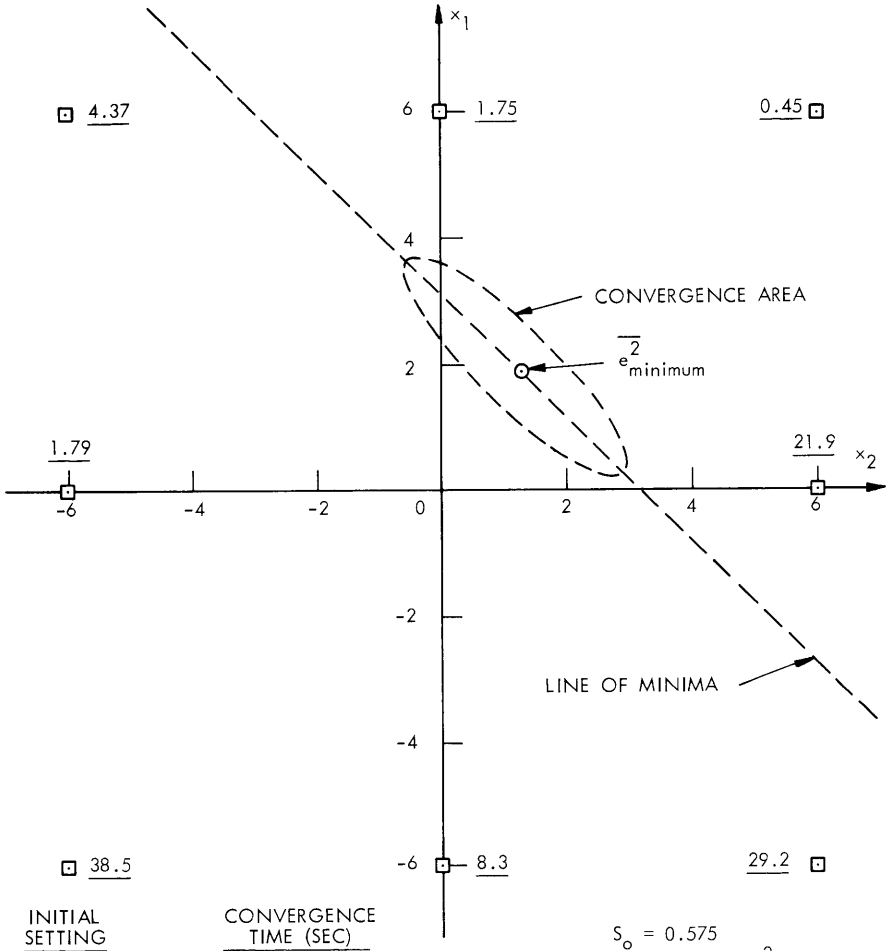

INITIAL SETTING	CONVERGENCE TIME (SEC)
(6, -6)	4.37
(6, 0)	1.75
(6, 6)	0.45
(0, -6)	1.79
(0, 6)	21.9
(-6, -6)	38.5
(-6, 0)	8.30
(-6, 6)	29.2

Fig. XIV-15. Convergence times from various initial settings of x_1 and x_2.

area, convergence times from various initial settings of the x_i, and the line of minima (the major axis of the ellipsoids of constant mean-square error plotted against the x_i). It is seen that the system takes very little time to reach the line of minima but takes the majority of the convergence time to move down the valley along the line of minima. For instance, if we look at the two points (-6,6) and (0,6), we see that the convergence time is approximately the same from both points, but that a slightly longer time is taken by the movement from the initial setting that is farthest from the line of minima. Looking at the two points (6,0) and (6,-6), we see that the perpendicular distance to the line of minima is approximately the same, but that for the initial setting farthest from the convergence area the convergence time is approximately one-third longer compared with the nearer setting.

A seeming deviation from this analysis is present if one considers the points (6,6) and (-6,-6). There the discrepancy is due to an overshoot when (-6,-6) is the starting point which does not occur when (6,6) is the starting point. (An example of the convergence process with overshoot is shown in Fig. XIV-16.) The range in convergence times from 0.45 second to 38.5 seconds is not indicative of the best possible performance of the system, since all of these runs were obtained with that value of D and A' which gave minimum convergence time from (6,6).

Figure XIV-17 shows the minimum mean-square error, the experimentally measured mean-square error, and the mean-square error calculated for the experimentally determined x_i, as a function of noise power with fixed desired output power for a 30-db range of noise power. Throughout the range the experimental and theoretical results agree quite closely, and thus indicate the capability of the adjustment procedure to operate properly over this wide range.

It was found in the four-filter case that the error on completion of optimization is approximately 40 per cent less than that obtainable with two filters. This is to be expected, since with more filters we can more closely approximate the spectrum of the desired signal.

5. Conclusions

We have shown that the adjustment procedure does produce the desired results for the mean-square error criterion. The time taken to converge can be controlled by proper setting of the adjustment procedure parameters. Since convergence times of well under 30 seconds can be obtained with this system and the system does perform satisfactorily over the required 30-db range in noise power density, it is applicable for use as an adaptive filter system in a radio communications link in which the background noise varies widely but remains approximately constant for a quarter of an hour or longer. Furthermore, it can be shown that the over-all gain in performance over a fixed filter which can be achieved by even this simple example is of the order of 5 db

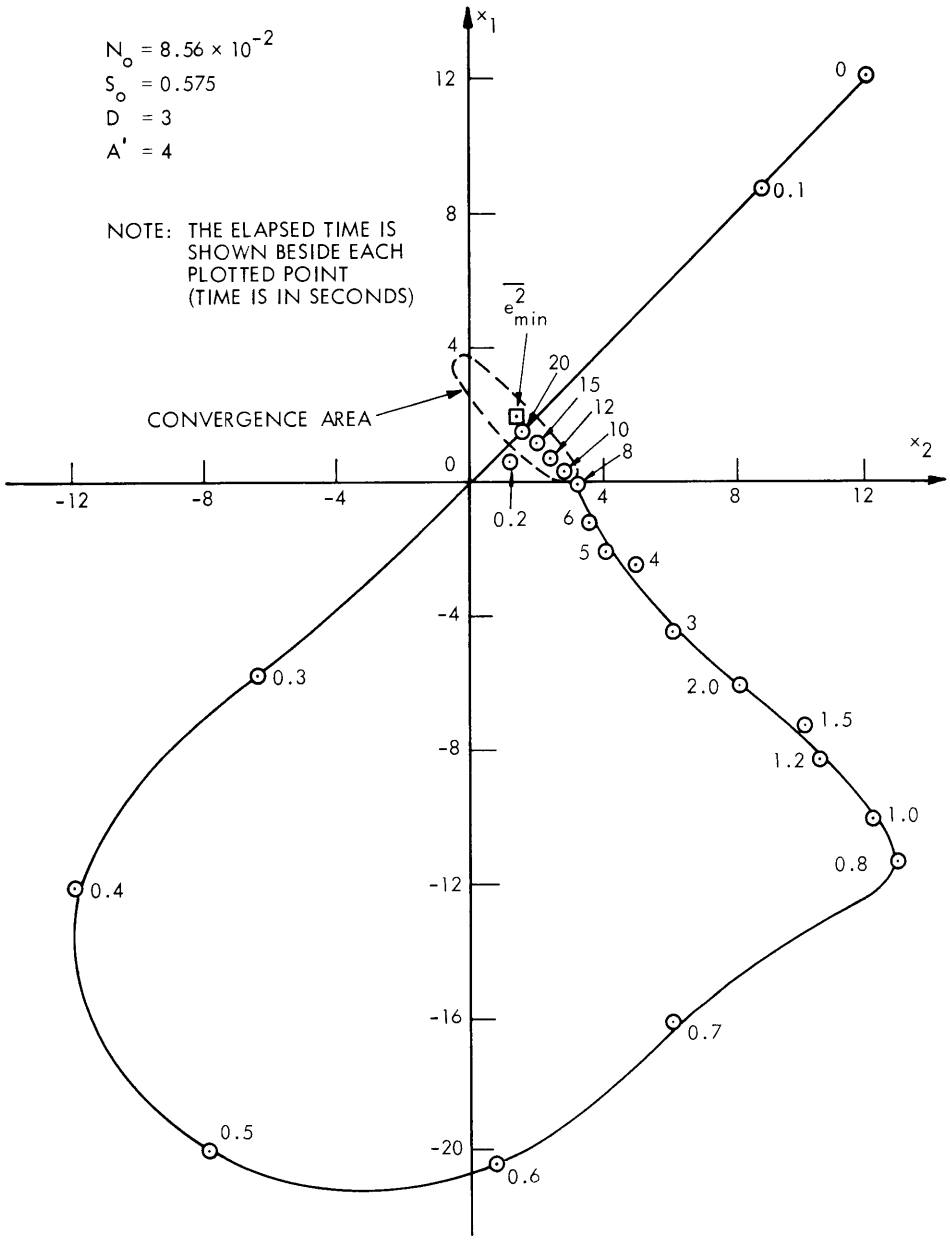

Fig. XIV-16. Typical convergence of the x_i (with overshoot).

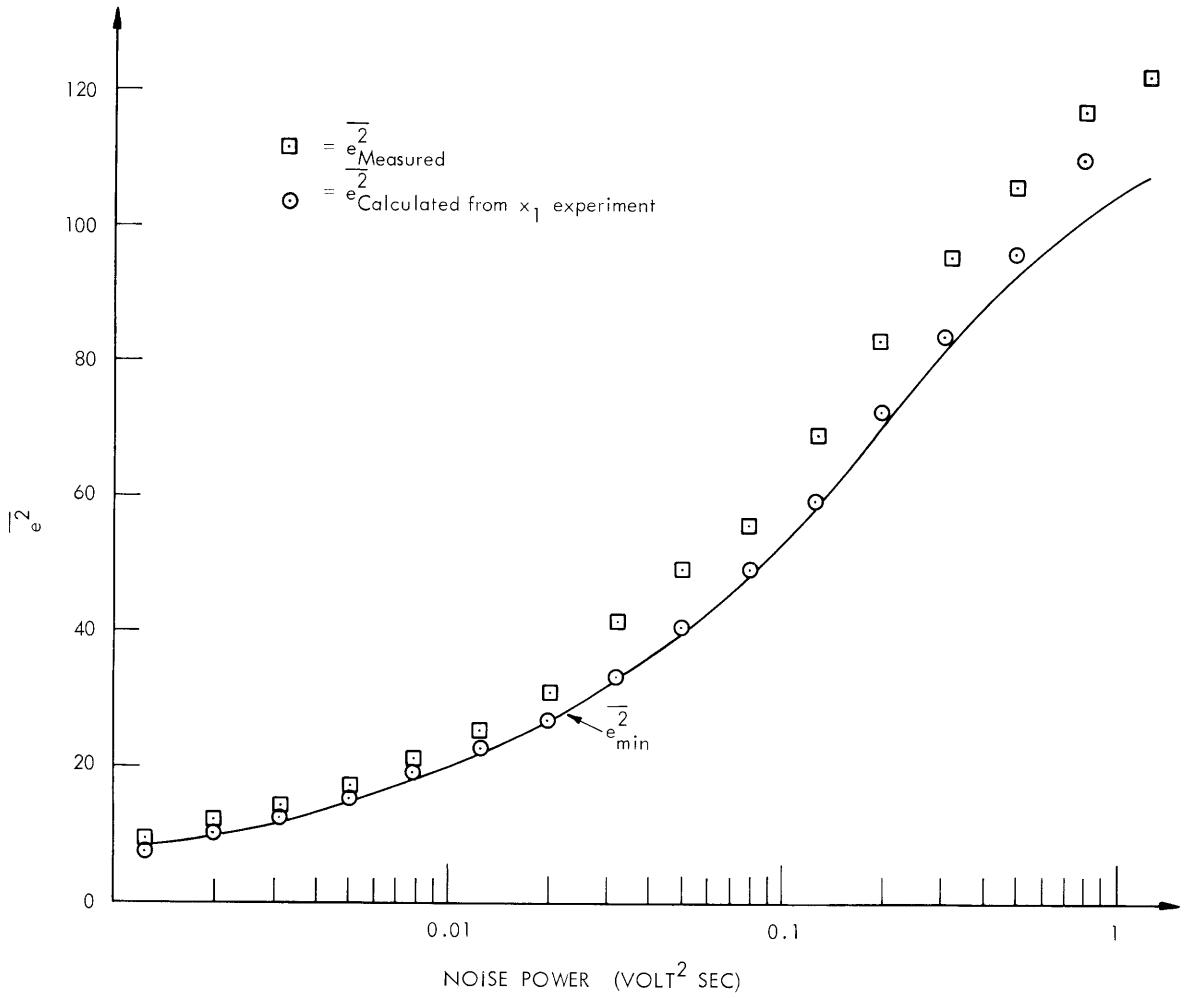

Fig. XIV-17. $\overline{e^2}_{measured}$, $\overline{e^2}_{minimum}$ and $\overline{e^2}_{calculated\ from\ x_i\ experiment}$ versus noise power for $S_o = 0.79$ volt^2 sec.

for a 14-db deviation of the noise power density from the value used for the fixed filter design.

A detailed description of these results has been given in the author's thesis.[4]

W. S. Smith, Jr.

References

1. D. J. Sakrison, Design of filters for non mean-square-error performance criteria by means of a continuous adjustment procedure, Quarterly Progress Report No. 66, Research Laboratory of Electronics, M. I. T., July 15, 1962, pp. 189-201; Quarterly Progress Report No. 67, October 15, 1962, pp. 119-126.

2. G. Fant, Acoustic Theory of Speech Production (Mouton and Company, The Hague, 1961).

3. D. J. Sakrison, An iterative method for the design of filters for non-mean-square error criteria, IEEE Trans. on Information Theory (in press).

4. W. S. Smith, Jr., An Adaptive Filter System for Radio Communications, S. M. Thesis, Department of Naval Architecture, M. I. T., May 17, 1963.

F. STUDY OF PHASE MODULATION WITH A GAUSSIAN SIGNAL

1. Introduction

The problem of determining the power density spectrum of a randomly phase-modulated sinusoid has been of interest not only in information transmission but also in the study of the problem of many coupled oscillators. Wiener has studied this problem and has derived the spectrum in closed form for a modulating signal that is a Gaussian process.[1] He obtained this result by using the set of orthogonal functionals that he derived, the "G-functionals."

Since the publication of his work, no experimental testing of the theory has been carried out. Therefore from the results obtained by Schetzen[2,3] an experiment was prepared in which the power density spectrum of a phase-modulated wave was studied by using the Wiener derivations.

Wiener has shown[1] that it is possible to obtain a power density spectrum with a dip in it if the modulating signal is the white Gaussian noise response of a quadratic filter. It is shown here that it is possible to obtain a dip in the spectrum by using a linear filter.

2. Theoretical Determination of the Power Density Spectrum[4]

Figure XIV-18 shows the general phase-modulation system. The input to the system, x(t), is white Gaussian noise with zero mean and a power density spectrum $\Phi_{xx}(\omega) = 1/2\pi$. The system with impulse response h(t) is a linear time-invariant system, and the signal s(t) is therefore a Gaussian signal. The amplifier m is merely used to adjust the rms level of g(t). The oscillator output, $f_c(t)$, is phase-modulated by g(t).

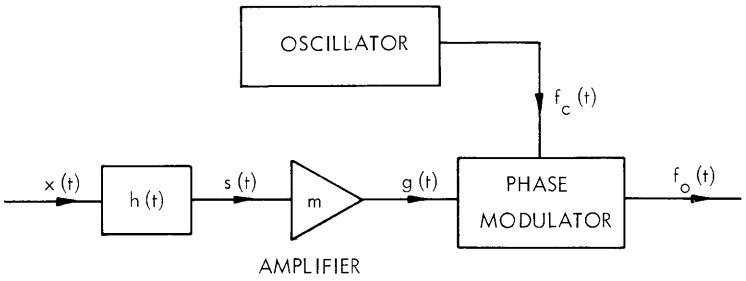

Fig. XIV-18. Phase-modulation system.

By the definition of phase modulation, if $f_c(t) = \cos \omega_c t$, then

$$f_o(t) = \cos (\omega_c t + g(t)). \tag{1}$$

We shall investigate the power density spectrum of $f_o(t)$. If we define a time signal $v(t) = e^{jg(t)}$, then $\psi_{oo}(\tau)$, the autocorrelation of $f_o(t)$, can be written in terms of $\psi_{vv}(\tau)$, the autocorrelation of $v(t)$,

$$\psi_{oo}(\tau) = \frac{1}{4}\left\{e^{-j\omega_c\tau}\psi_{vv}(\tau) + e^{j\omega_c\tau}\psi^*_{vv}(\tau)\right\}. \tag{2}$$

Using the set of G-functionals and the techniques developed by Wiener,[1] we can put $\psi_{oo}(\tau)$ into a form that has an easily derived Fourier transform. The easiest way to do this is to express $g(t)$ in terms of $x(t)$. With respect to Fig. XIV-18

$$s(t) = \int_{-\infty}^{\infty} h(t-\sigma)\, x(\sigma)\, d\sigma. \tag{3}$$

Let us normalize $h(t)$ by letting

$$h(t) = k\phi(t) \tag{4}$$

where $k^2 = \int_{-\infty}^{\infty} h^2(t)\, dt$. By defining $b = mk$, $g(t)$ can be written

$$g(t) = b\int_{-\infty}^{\infty} \phi(t-\sigma)\, x(\sigma)\, d\sigma. \tag{5}$$

Wiener[1] has expanded $\psi_{vv}(\tau)$, the autocorrelation of $v(t)$, in terms of the G-functionals:

$$\psi_{vv}(\tau) = e^{-b^2}\sum_{n=0}^{\infty}\frac{b^{2n}}{n!}\left[\int_{-\infty}^{\infty}\phi(t)\,\phi(t+\tau)\,dt\right]^n. \tag{6}$$

Because of the special form of this expansion, it can be simplified. Defining

$$\psi_{\phi\phi}(\tau) = \int_{-\infty}^{\infty}\phi(t)\,\phi(t+\tau)\,dt, \tag{7}$$

we obtain

$$\psi_{vv}(\tau) = \exp\left\{-b^2[1-\psi_{\phi\phi}(\tau)]\right\}. \tag{8}$$

Since $\psi_{vv}(\tau)$ is pure real, (2) can be written

$$\psi_{oo}(\tau) = \frac{1}{2}\psi_{vv}(\tau)\cos\omega_c\tau. \tag{9}$$

The spectrum of $\psi_{oo}(\tau)$ is merely the spectrum of $\frac{1}{4}\psi_{vv}(\tau)$ centered at the frequencies $\omega = \pm\omega_c$.

In order to simplify measurements, as well as calculations, it is desirable to set $\omega_c = 0$. This is merely a shift of the spectrum to a center frequency of $\omega = 0$. Notice that this forces the spectrum of $\psi_{oo}(\tau)$ to be symmetric. We then have

$$\psi_{oo}(\tau) = \frac{1}{2}\psi_{vv}(\tau). \tag{10}$$

The desired power density spectrum, $\Psi_{oo}(j\omega)$, is the Fourier transform of $\psi_{oo}(\tau)$. This can be written by expressing $\psi_{vv}(\tau)$ as a sum and interchanging the order of the sum and the integral,

$$\Psi_{oo}(j\omega) = \frac{1}{2}e^{-b^2}\sum_{n=0}^{\infty}\frac{b^{2n}}{n!}\frac{1}{2\pi}\int_{-\infty}^{\infty}\psi_{\phi\phi}^{n}(\tau)\,e^{-j\omega\tau}\,d\tau. \tag{11}$$

Since $\psi_{\phi\phi}(\tau)$ is an even function in τ, it can be represented as follows:

$$\psi_{\phi\phi}(\tau) = \begin{cases} \displaystyle\sum_{k=-\infty}^{\infty} A_k e^{s_k\tau} & \text{for } \tau \geqslant 0 \\ \displaystyle\sum_{k=-\infty}^{\infty} A_k e^{-s_k\tau} & \text{for } \tau < 0. \end{cases} \tag{12}$$

Defining $\psi_{\phi\phi_1}(\tau) = \psi_{\phi\phi}(\tau)$ for $\tau \geqslant 0$ and $\psi_{\phi\phi_2}(\tau) = \psi_{\phi\phi}(\tau)$ for $\tau < 0$ and both functions zero otherwise, we have

$$\psi_{\phi\phi}(\tau) = \psi_{\phi\phi_1}(\tau) + \psi_{\phi\phi_2}(\tau) \tag{13}$$

and

$$\psi_{\phi\phi}^{n}(\tau) = \psi_{\phi\phi_1}^{n}(\tau) + \psi_{\phi\phi_2}^{n}(\tau). \tag{14}$$

Defining $\Psi_1^{(n)}(s)$ and $\Psi_2^{(n)}(s)$ as the exponential transforms of $\psi_{\phi\phi_1}^{n}(\tau)$ and $\psi_{\phi\phi_2}^{n}(\tau)$, respectively, we can write

$$\Psi_1^{(n)}(s) = \sum_{k_1=-\infty}^{\infty}\sum_{k_2=-\infty}^{\infty}\cdots\sum_{k_n=-\infty}^{\infty}\frac{A_{k_1}A_{k_2}\cdots A_{k_n}}{\left(s-s_{k_1}-s_{k_2}-\cdots-s_{k_n}\right)}, \qquad \text{if } \operatorname{Re}(s) > \sum_{i=1}^{n}\operatorname{Re}\left(s_{k_i}\right) \tag{15}$$

and

$$\Psi_2^{(n)}(s) = \sum_{k_1=-\infty}^{\infty} \sum_{k_2=-\infty}^{\infty} \cdots \sum_{k_n=-\infty}^{\infty} \frac{(-1)A_{k_1} A_{k_2} \cdots A_{k_n}}{\left(s+s_{k_1}+s_{k_2}+\ldots+s_{k_n}\right)}, \qquad \text{if } \operatorname{Re}(s) < -\sum_{i=1}^{n} \operatorname{Re}\left(s_{k_i}\right). \tag{16}$$

Notice that the conditions on Re (s) are satisfied if the Fourier transform $\psi_{\phi\phi}(\tau)$ exists; this existence is assured by the Wiener theorem.[5]

In order to interpret these sums, it is convenient to relate them to an example. This example is the one that was used in the actual experiment and will be discussed in parallel with the rest of the derivation.

Let the only nonzero values for A_k in the expansion of $\psi_{\phi\phi}(\tau)$ be those for which $k = +1$ and $k = -1$. We then have

$$\psi_{\phi\phi_1}(\tau) = \begin{cases} A_1 e^{s_1\tau} + A_{-1} e^{s_{-1}\tau}; & \tau \geq 0 \\ 0; & \tau < 0. \end{cases} \tag{17}$$

From Eq. 15

$$\Psi_1^{(1)}(s) = \sum_{k_1=-1}^{1} \frac{A_{k_1}}{\left(s-s_{k_1}\right)} = \frac{A_1}{s-s_1} + \frac{A_{-1}}{s-s_{-1}} \tag{18}$$

$$\Psi_1^{(2)}(s) = \sum_{k_1=-1}^{1} \sum_{k_2=-1}^{1} \frac{A_{k_1} A_{k_2}}{\left(s-s_{k_1}-s_{k_2}\right)} = \frac{A_1 A_1}{s-2s_1} + \frac{2A_1 A_{-1}}{s-s_1-s_{-1}} + \frac{A_{-1}A_{-1}}{s-2s_{-1}}. \tag{19}$$

These two expressions, $\Psi_1^{(1)}(s)$ and $\Psi_1^{(2)}(s)$, are shown in Fig. XIV-19 in which the poles and residues (in parentheses) of each of the terms in the respective expressions are plotted in the s-plane. Notice that s_1 and s_{-1} are chosen to be a complex-conjugate pair, which they must be for a real autocorrelation function; this fact is represented by defining

$$s_1 = -\alpha + j\omega_o; \qquad s_{-1} = -\alpha - j\omega_o. \tag{20}$$

Notice that it is possible to consider $\Psi_1^{(2)}(s)$ the result of a two-dimensional convolution of $\Psi_1^{(1)}(s)$ with $\Psi_1^{(1)}(s)$ in the s-plane. The term two-dimensional convolution is meant to imply that the coordinates of each pole in the s-plane are found by a one-dimensional convolution along the respective coordinate.

The quantity $\Psi_1^{(3)}(s)$ is found to be

$$\Psi_1^{(3)}(s) = \frac{A_1^3}{(s-3s_1)} + \frac{3A_1^2A_{-1}}{(s-2s_1-s_{-1})} + \frac{3A_1A_{-1}^3}{(s-s_1-2s_{-1})} + \frac{A_{-1}^3}{(s-3s_{-1})}, \tag{21}$$

which again can be recognized as the two-dimensional convolution of $\Psi_1^{(1)}(s)$ and $\Psi_1^{(2)}(s)$ in the s-plane.

In general, the expression $\Psi_1^{(n)}(s)$ is the result of a two-dimensional convolution of $\Psi_1^{(1)}(s)$ with $\Psi_1^{(n-1)}(s)$.

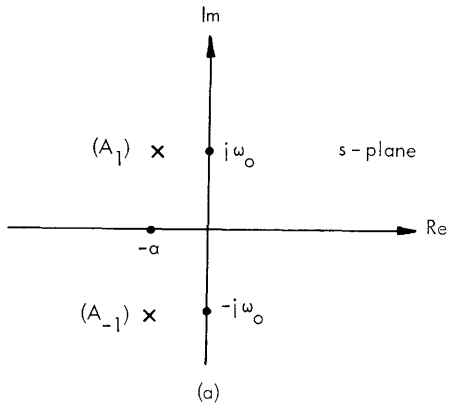

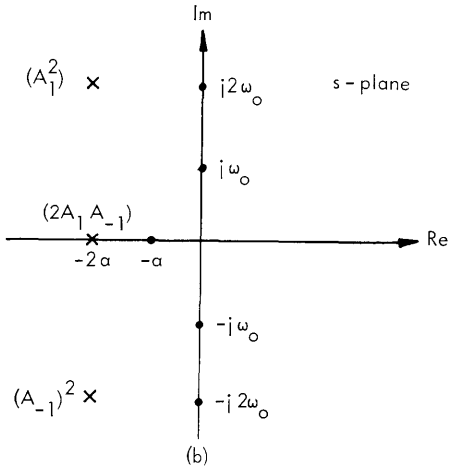

Fig. XIV-19. (a) $\Psi_1^{(1)}(s)$.
(b) $\Psi_1^{(2)}(s)$.

The representation of $\Psi_2^{(n)}(s)$ in the s-plane can be derived from $\Psi_1^{(n)}(s)$ by noticing that each of the poles appears at a point in the s-plane that is symmetric about $s = 0$ and the residue of the pole is the negative of the residue of the respective pole of $\Psi_1^{(n)}(s)$, as can be seen from Eqs. 15 and 16.

Although the example shown has only two nonzero A_k, it is easily seen that the technique, including the two-dimensional convolution, is valid in the general case.

Rewriting Eq. 11 in terms of the exponential transform, we have

$$\Psi_{oo}(s) = \frac{1}{2} e^{-b^2} \sum_{n=0}^{\infty} \frac{b^{2n}}{n!} \int_{-\infty}^{\infty} \left[\psi^n_{\phi\phi_1}(\tau) + \psi^n_{\phi\phi_2}(\tau)\right] e^{-s\tau}\, d\tau \tag{22}$$

$$\Psi_{oo}(s) = \frac{1}{2} e^{-b^2} \sum_{n=0}^{\infty} \frac{b^{2n}}{n!} \left[\Psi_1^{(n)}(s) + \Psi_2^{(n)}(s)\right]. \tag{23}$$

Since $\Psi_1^{(n)}(s)$ and $\Psi_2^{(n)}(s)$ have already been derived, Eq. 23 corresponds only to summing with the given weighting.

$\Psi_{oo}(s)$ can be represented by plotting the poles and residues of each of the respective terms in the s-plane.

In the example, in which the only nonzero terms are those containing only A_1 and A_{-1}, the poles and residues are found from the result above. In Fig. XIV-20 the terms of $\Psi_{oo}(s) \cdot 2e^{b^2}$ are plotted for values of n from 1 to 4. The higher terms are easily obtained by the two-dimensional technique and by multiplying the result by $b^{2n}/n!$. The term for $n = 0$ corresponds to an impulse at $\omega = 0$ and is omitted.

The power density spectrum of $f_o(t)$ is the Fourier transform of $\psi_{oo}(\tau)$, or $\Psi_{oo}(j\omega)$. This expression is obtained by replacing s by $j\omega$ in $\Psi_{oo}(s)$ and then multiplying by $1/2\pi$ to conform to the common definition of the Fourier transform.

$$\Psi_{oo}(j\omega) = \frac{1}{2\pi} \cdot \frac{1}{2} \cdot e^{-b^2} \sum_{n=0}^{\infty} \frac{b^{2n}}{n!} \left[\Psi_1^{(n)}(j\omega) + \Psi_2^{(n)}(j\omega)\right]. \tag{24}$$

$\Psi_{oo}(j\omega)$ can be obtained from s-plane representation. Except for a multiplicative constant, $\Psi_{oo}(j\omega)$ can be obtained by taking the reciprocal of the vector from the pole of a term of $\Psi_{oo}(s)$ to the point $s = j\omega$ times the residue of that pole and summing these results over all poles.

Notice that this is quite different from the normal s-plane technique of finding the product of the vectors from the zeros divided by the product of the vectors from the poles. An attempt was made to find $\Psi_{oo}(s)$ as a ratio of products of the form $(s-s_i)/(s-s_j)$. This attempt was not successful in the general case, because of the complexity arising from the infinite number of poles.

In any specific case it is not necessary to complete the sum in Eq. 24 because the factor $b^{2n}/n!$ approaches zero rapidly as n becomes large. The size of n needed depends on the value of b^2 and the degree of accuracy desired in $\Psi_{oo}(j\omega)$.

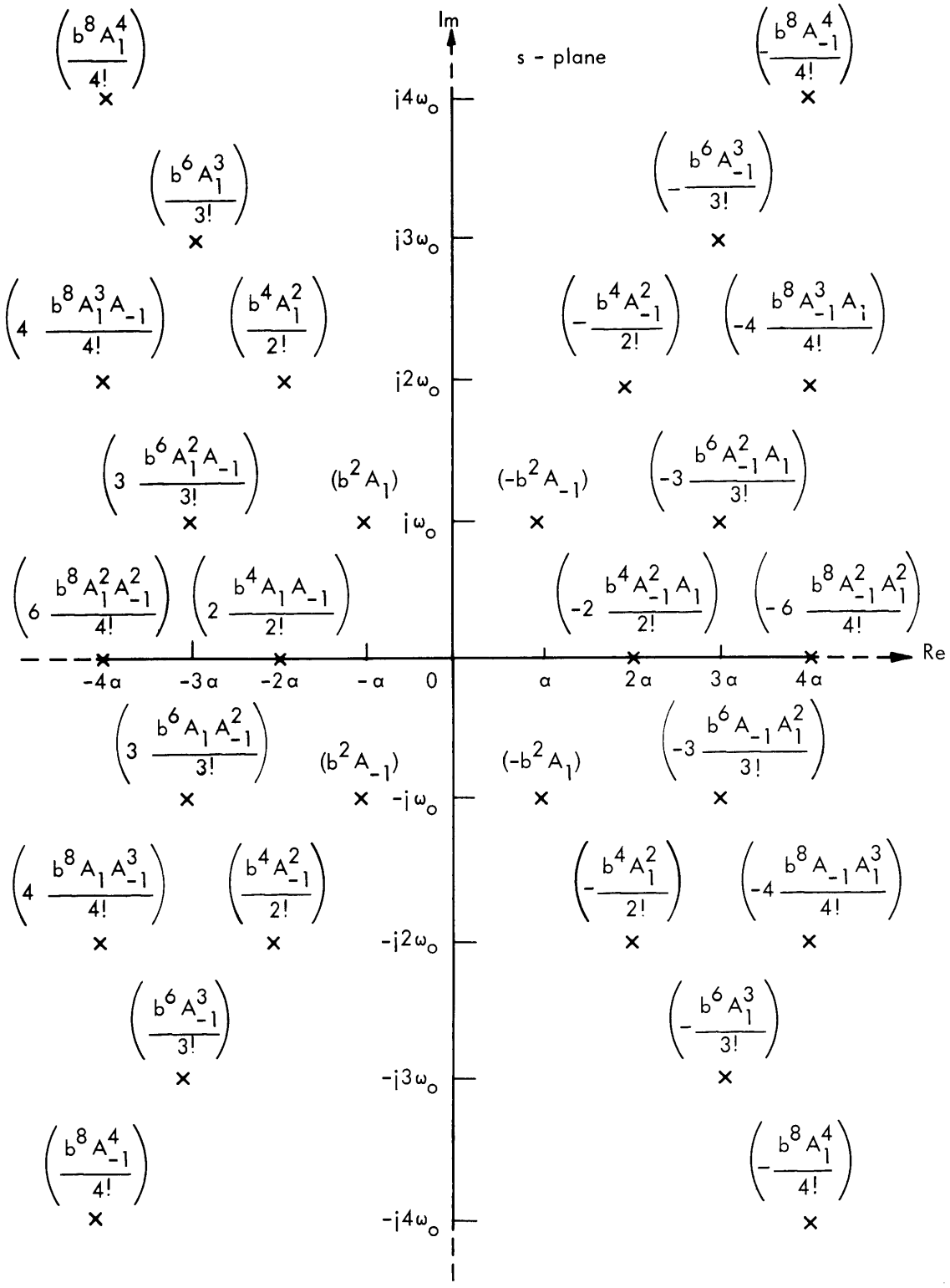

Fig. XIV-20. Terms of $2e^{b^2}\Psi_{oo}(s)$.

Because of the simplicity of Eq. 24 it is a relatively simple matter to program a computer to calculate the sum for any arbitrary filter autocorrelation function. This program is now being developed at the Computation Center of the Massachusetts Institute of Technology.

3. Experiment

a. Experimental Procedure

The block diagram of the experimental system is shown in Fig. XIV-21.

The sinusoid $f_c(t)$ is phase-modulated by s(t) which is the output of a shaping filter whose input is white Gaussian noise. The output of the phase modulator, $f_1(t)$, has a spectrum centered about the frequency of $f_c(t)$. In order to facilitate measurements of the spectrum it was desirable to center this spectrum about zero frequency, which is equivalent to setting the frequency of $f_c(t)$ equal to zero. This was accomplished in

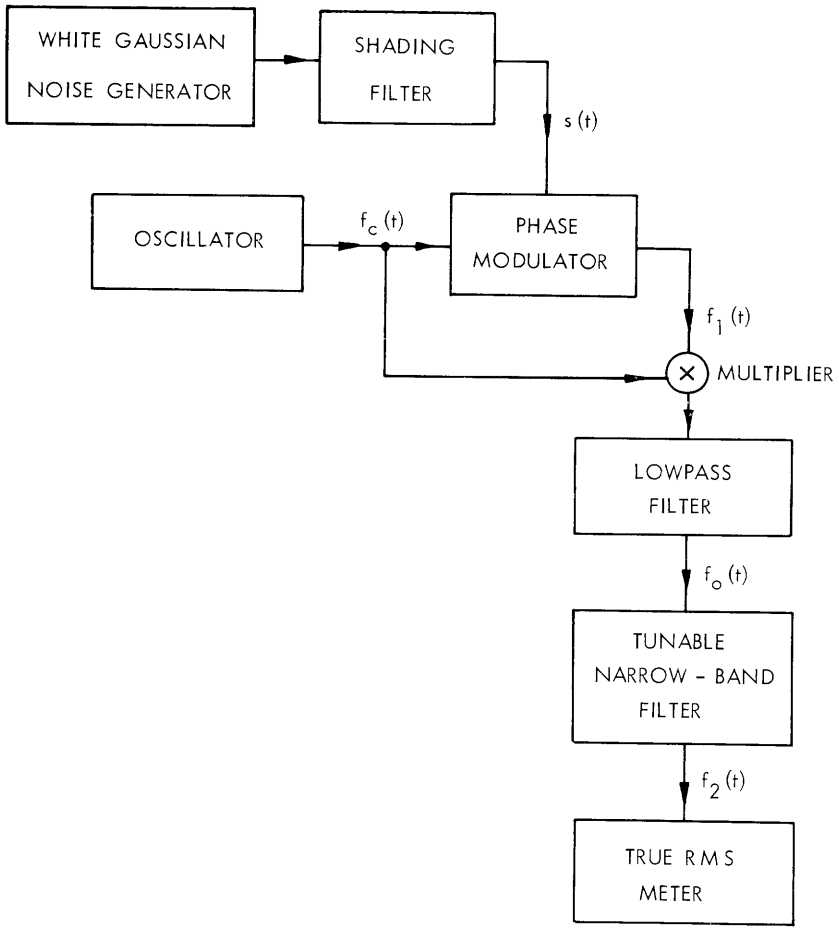

Fig. XIV-21. Experimental system.

practice by multiplying $f_1(t)$ by $f_c(t)$ and eliminating the double-frequency components with a lowpass filter. The power density spectrum of $f_o(t)$ was measured by passing $f_o(t)$ through a narrow-band filter and measuring the output on a true rms meter.

b. Implications of the Theory on Design

In order to verify the theory experimentally it was necessary to synthesize a filter that was such that when the response of this filter to white Gaussian noise was used as a signal to phase-modulate a sinusoid, the resulting power density spectrum would be easily recognizable. In order to keep the calculational difficulties to a minimum, it was desirable to use a filter with only two nonzero values of A_k in the expansion of the autocorrelation of its impulse response, as in the example used in the theoretical derivation. The resulting power density spectrum of the phase-modulated wave can then be obtained from Fig. XIV-20 by taking the reciprocal of the vector from a pole to the frequency under consideration times the residue at that pole and summing these results over all poles. From Fig. XIV-20 it can be seen that if the ratio of ω_o/α is large and if b is chosen to be approximately one, the dominant terms at $\omega = 0$ will be from the poles at $s = \pm 2\alpha$ and the dominant terms at $\omega = \omega_o$ will be from the poles at $s = \pm\alpha + j\omega_o$. Under these conditions, it is possible to have a power density spectrum that has a dip between $\omega = 0$ and $\omega = \omega_o$.

Since this power density spectrum has the property of being easily recognizable and has implications in the study of coupled oscillators, as shown by Wiener[1] and Schetzen,[2] a filter was designed to give this dip.

In order to make the dip in the power density spectrum prominent, it is desirable to have the magnitude at $\omega = 0$ approximately the same as the magnitude at $\omega = \omega_o$. In order to satisfy this condition, the following relation must be satisfied:

$$\frac{b^2 A_1}{\alpha} \approx \frac{2b^4 A_1 A_{-1}}{2!\, 2\alpha}. \tag{25}$$

It will be shown that the magnitudes of A_1 and A_{-1} are approximately 1/2. In that case

$$b \approx 2. \tag{26}$$

The symbol, b, is the product of the normalization constant of the filter and the gain of the phase modulator. The instantaneous phase of the phase-modulated signal under consideration can be expressed as Eq. 5. Since x(t) is defined as white Gaussian noise with zero mean and a power density spectrum of $1/2\pi$, the mean of g(t) is zero and the variance of g(t) is equal to b^2.

According to Eq. 25 it is desirable to have $b \approx 2$, which implies a variance of 4 in the phase of $f_o(t)$. This then puts a difficult design constraint on the phase modulator,

since the phase must be able to swing plus or minus three times the standard deviation. The phase modulator must swing $\pm 3 \times 2 \times 57.3$ degrees or a total swing of approximately 700 degrees. If the value of the power density spectrum at $\omega = 0$ is allowed to be one-fourth the value at $\omega = \omega_o$, b could be reduced to 1, which would reduce the necessary swing in phase to 350 degrees. Most phase-modulation systems in use have a linear swing in phase of less than 90 degrees. Since a value of b greater than 1 was desired, a phase modulator had to be constructed with a swing of at least 360 degrees.

The autocorrelation function of the impulse response of the filter should have poles located at $s = \pm a \pm j\omega_o$. If the Fourier transform of a filter is $H(j\omega)$, then the Fourier transform of its autocorrelation function is $|H(j\omega)|^2$. It is easily seen, then, that the desired filter has poles at $s = -a \pm j\omega_o$. A filter with these poles is easily constructed by a parallel connection of a resistor, an inductor, and a capacitor. The input to the filter must be a current and the output a voltage.

c. Component Parts

The major part of this experiment was the design and construction of the phase modulator because of the range required. The description of the phase modulator is explained in detail in the author's thesis,[4] together with a description of the other component parts, which are shown in Fig. XIV-21.

d. Operational Data

The frequency of the sinusoid $f_c(t)$ in Fig. XIV-21 was 1500 kc. The modulating signal, g(t), was bandlimited so that there were no frequency components above 20 kc. The phase modulator could operate at well above this frequency.

Figure XIV-22 shows the experimental plot of the phase angle of the 1500-kc sinusoid versus the input-modulating voltage. The curve is very linear. It is at all points within 0.8 per cent of the best straight line drawn through the points. The curve levels off after ±3.5 volts as a result of Zener diodes used in the construction.[4]

Because of the design of the phase modulator, the output signal is free of amplitude modulation.

The rms value of the input voltage was adjusted to be 1 volt. Since the cutoff voltage of the phase modulator is 3.5 volts, 99.9 per cent of the time the input voltage was in the linear range of the phase modulator. For this reason the probability density of the phase could be considered to be pure Gaussian.

The shaping filter had a resonant frequency of 8.3 kc and a Q of 13.5. For that reason the spectrum of the Gaussian noise generator which was level between 20 cps and 20 kc was considered white for the purposes of this experiment.

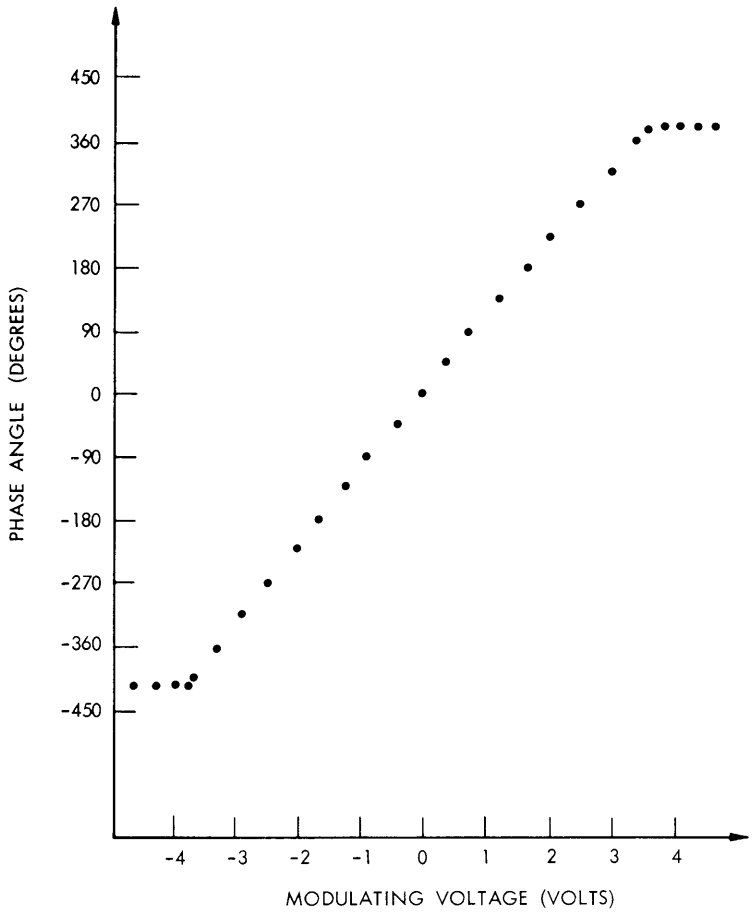

Fig. XIV-22. Phase angle of sinusoid versus input modulating voltage.

4. Comparison of Theoretical and Experimental Results

The system function of a parallel RLC circuit as described in section 3 is merely the impedance. The system function, H(s), therefore is

$$H(s) = \frac{s/C}{s^2 + \frac{s}{RC} + \frac{1}{LC}}. \tag{27}$$

By defining $a = 1/RC$, $\omega_o = 1/\sqrt{LC}$, $\omega_d = \sqrt{\omega_o^2 - a^2}$, the normalized autocorrelation function of the impulse response of the system, $\psi_{\phi\phi}(\tau)$, is

$$\psi_{\phi\phi}(\tau) = \frac{1}{2}\left(1 + j\frac{a}{\omega_d}\right)\exp[-(a-j\omega_d)|\tau|] + \frac{1}{2}\left(1 - j\frac{a}{\omega_d}\right)\exp[-(a+j\omega_d)|\tau|]. \tag{28}$$

In the notation of the example discussed in section 2, $A_1 = \frac{1}{2}\left(1 + j\frac{a}{\omega_d}\right)$, $A_{-1} = \frac{1}{2}\left(1 - j\frac{a}{\omega_d}\right)$,

$s_1 = -\alpha + j\omega_d$, and $s_{-1} = -\alpha - j\omega_d$.

As stated in section 2, the power density spectrum of the phase-modulated wave, $f_o(t)$, is obtained by means of Fig. XIV-20. This is obtained by taking the reciprocal of the vector from a pole to the frequency under consideration times the residue at that pole and summing over all poles. Consider one of the poles in Fig. XIV-20 and its mirror reflection across the imaginary axis. If a vector is drawn from each of these poles to a point on the imaginary axis, both vectors will have the same imaginary component and the real components will be negatives of each other. Because of this fact and since the residues of these poles are the negative complex conjugates of each other, the sum of the contributions from this pair of poles will be twice the real part of the contribution from either one of the poles. For this reason it is possible to consider only one-half of the poles, say the poles in the left-half plane, by taking twice the real part of each contribution.

Figure XIV-23 shows the notation used to designate the contributions from each of the specific poles. The sum contribution from the poles at $s = \pm n\alpha + jm\omega_d$ is labeled CUnm and the contribution from the poles at $s = \pm n\alpha - jm\omega_d$ is labeled CLnm. CU11 is therefore the sum contribution from the poles at $s = \pm\alpha + j\omega_d$ or twice the real part of the contribution from the pole at $s = -\alpha + j\omega_d$.

$$CU11 = \frac{1}{2\pi} \cdot \frac{1}{2} e^{-b^2} 2\mathrm{Re} \frac{b^2 A_1}{(j\omega+\alpha-j\omega_d)} = \frac{1}{2\pi} \cdot \frac{1}{2} e^{-b^2} \frac{b^2 \left[\alpha + \frac{\alpha}{\omega_d}(\omega-\omega_d)\right]}{\alpha^2 + (\omega-\omega_d)^2}. \tag{29}$$

The contribution from the poles at $s = \pm\alpha - j\omega_d$ is

$$CL11 = \frac{1}{2\pi} \cdot \frac{1}{2} e^{-b^2} \frac{b^2 \left[\alpha - \frac{\alpha}{\omega_d}(\omega+\omega_d)\right]}{\alpha^2 + (\omega+\omega_d)^2}. \tag{30}$$

The contribution from the poles at $s = \pm 2\alpha + j2\omega_d$ is

$$CU22 = \frac{1}{2\pi} \cdot \frac{1}{2} e^{-b^2} 2\mathrm{Re} \frac{\frac{b^4}{2!} A_1^2}{j\omega + 2\alpha - j2\omega_d} = \frac{1}{2\pi} \cdot \frac{1}{2} e^{-b^2} \frac{b^4}{4} \frac{\left[2\alpha\left(1 - \frac{\alpha^2}{\omega_d^2}\right) + \frac{2\alpha}{\omega_d}(\omega-\omega_d)\right]}{4\alpha^2 + (\omega-\omega_d)^2}. \tag{31}$$

The contributions from other poles are derived in the same manner and will not be listed here.

The number of poles to be considered in any one case depends on the accuracy desired in $\Psi_{oo}(j\omega)$ and in the values of b, α, and ω_d.

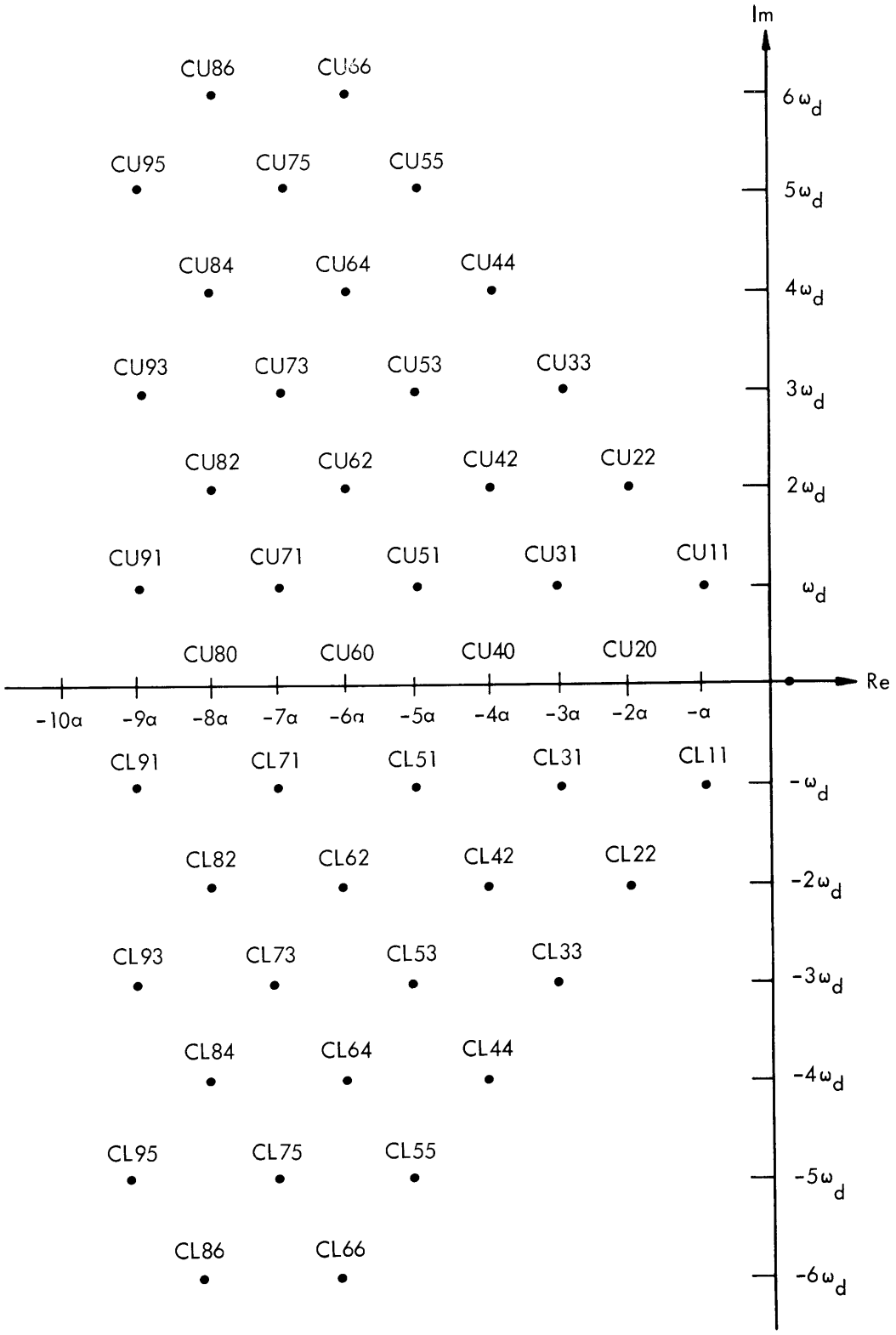

Fig. XIV-23. Notation used to designate contributions from each of the specific poles.

The value of b is the standard deviation of phase of $f_1(t)$ in radians. The measured rms value of the signal, s(t), applied to the phase modulator in this experiment was 1.05 volts. The standard deviation of the phase can be obtained from the phase versus voltage curve, Fig. XIV-22. The slope of this curve is 105 degrees per volt. Therefore the standard deviation is $(1.05)\cdot(105) = 110.3$ degrees or 1.926 radians, and the value of b used in the calculations is 1.926. The measured Q of the filter was 13.5, which yields a value of 27 for the ratio ω_d/α. The measured resonance of the filter was 8.3 kc; therefore $\omega_d \approx 2\pi \cdot 8.3\times10^3$ radians per second and $\alpha = 1.930\times10^3$ nepers per second.

With these values of b, α, and ω_d used, the contributions from the various poles were calculated for some specific frequencies. The variable used in these calculations is f, where $\omega = 2\pi f$. These results are shown in Table XIV-1. Only the contributions from the largest poles are shown. The contributions from the other poles were too small to be of interest in the range of frequencies under consideration. The sum of these contributions, labeled CT in Table XIV-1, is plotted in Fig. XIV-24 as a solid line. It is important to notice that the values of b, α, and ω_d chosen do, indeed, produce the desired dip in the spectrum between $\omega = 0$ and $\omega = \omega_d$.

The experimental measurements were made by applying the phase-modulated signal, $f_o(t)$, to a narrow-band filter. The filter was tuned to the desired frequency and the output of the filter was measured on a true rms meter. The square of this measurement was recorded.

Even though the meter had an effective time constant of approximately 5 sec, the meter reading fluctuated back and forth a distance that was a sizable percentage of the average. In order to overcome this result of finite time integration, the meter reading was averaged by eye over several minutes. The results of these measurements are shown as bars superimposed over the theoretical curve in Fig. XIV-24. The length of the bar indicates the range in which the true average could lie on the basis of the measurements and the center is the estimated average value. Since the amplitude of the modulated sinusoid was not one, and since the gain of the narrow-band filter was not one, the absolute magnitude of the series of measurements was not known. For that reason the experimental curve was multiplied by a constant that seemed to yield the best overall fit to the theoretical curve.

Figure XIV-24 shows that the experimental data follow the theoretical curve very closely. It can be seen that both the experimental and the theoretical curves have the desired dip between $\omega = 0$ and $\omega = \omega_d$. It can be noted further that the dip occurs at the same place in both curves and that relative heights of the peaks also agree. In fact, there are only a few minor departures of the experimental curve from the theoretical curve.

Some possible explanations for these minor departures might be errors arising from

Table XIV-1. Contributions of the poles in Fig. XIV-23 at various frequencies in units of 10^{-9} watts per rad/sec.

F	CU11	CL11	CU22	CU20	CL22	CU31	CL31	CU42	CU40	CU51	CL51	CU62	CU60	CU71	CU80	CT
0	0	0	-2	3476	-2	17	17	0	1497	20	20	1	382	8	62	5495
500	0	0	-2	2092	-2	20	15	0	1284	22	17	1	356	9	59	3873
1000	1	0	-2	953	-2	24	13	0	901	26	15	1	295	11	53	2288
1500	1	-1	-2	500	-2	28	11	1	602	30	14	2	230	12	45	1470
2500	3	-1	-2	198	-2	41	9	1	292	42	11	2	135	17	30	774
3500	6	-1	-2	104	-2	62	7	2	164	61	9	3	83	23	20	539
4500	13	-1	-2	64	-2	101	5	3	104	95	7	3	55	34	14	493
5500	30	-1	-2	43	-2	187	4	4	71	160	6	4	39	54	10	606
6500	83	-1	-1	31	-2	414	3	6	52	299	5	5	28	87	8	1016
7000	167	-1	-1	27	-2	682	3	7	45	418	5	6	25	109	7	1495
7500	435	-1	-1	23	-2	1187	3	8	39	571	4	7	22	132	6	2433
8000	1848	-1	0	20	-2	1920	2	10	35	708	4	8	19	148	5	4723
8300	3743	-1	0	19	-2	2149	2	11	32	740	4	9	18	152	5	6880
9000	656	-1	1	16	-2	1402	2	14	27	623	3	11	15	139	4	2911
9500	264	-1	2	14	-2	836	2	17	25	473	3	13	14	118	4	1781
10500	91	-1	5	12	-2	350	1	25	20	256	3	18	11	77	3	868
11500	47	-1	10	10	-2	186	1	38	17	149	2	26	10	50	3	546

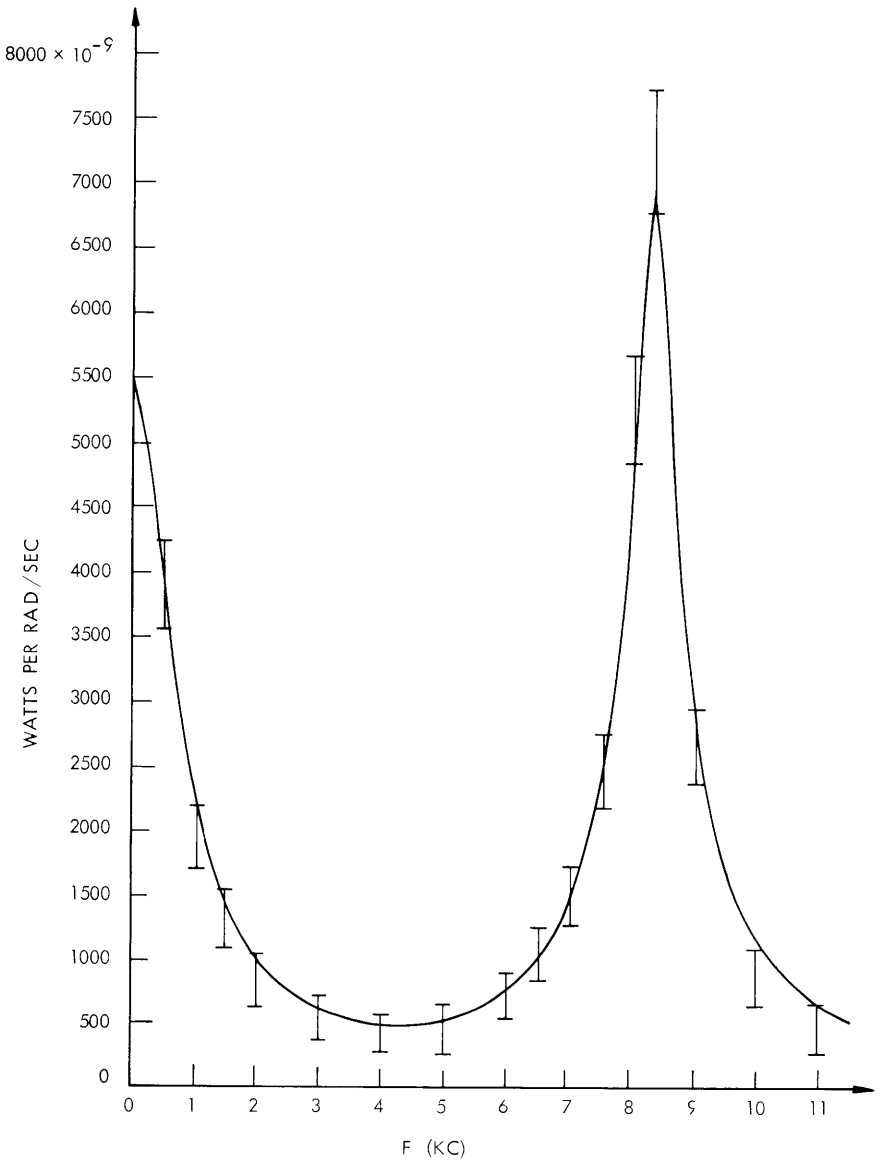

Fig. XIV-24. Theoretical and experimental curves.

the finite time averaging and possibly a value for b, the rms phase deviation, that is slightly in error and affects the spectrum greatly. Another possible explanation of the departures might be that the noise source is not a true Gaussian source. Even though lower-order moments are those of a true Gaussian source, departures in the higher-order moments would cause experimental errors.

It would be interesting to measure the power-density spectrum by using other values of b. As observed, a higher value of b would make stronger use of the higher moments of the noise waveform. Departures of the higher-order moments from those of a true

Gaussian wave would increase the discrepancy between the measured spectrum and the theoretical calculation because the latter is based on a true Gaussian source. These measurements could be used for checking the higher moments of a Gaussian source.

In many current studies, the power density spectrum of $e^{j\theta(t)}$, where $\theta(t)$ is a nonlinear operation on a Gaussian process, is of interest. The theoretical calculations in these studies become very complicated (see, for example, the calculations of Schetzen[2] in which the operation is the sum of a linear and a quadratic operation). The power density spectrum in these complicated cases could be obtained very easily by using the phase modulator described in the author's thesis.[4] The linear filter could be replaced by the desired nonlinear filter and the power density spectrum could be measured as described here.

J. K. Clemens

References

1. N. Wiener, Nonlinear Problems in Random Theory (The Technology Press of Massachusetts Institute of Technology, Cambridge, Mass., and John Wiley and Sons, Inc., New York, 1958).

2. M. Schetzen, Some Problems in Nonlinear Theory, Technical Report 390, Research Laboratory of Electronics, M. I. T., July 6, 1962.

3. M. Schetzen, Unpublished Notes, 1960.

4. J. K. Clemens, A Study of Phase-Modulation with a Gaussian Signal, S. M. Thesis, Department of Electrical Engineering, M. I. T., May 13, 1963.

5. Y. W. Lee, Statistical Theory of Communication (John Wiley and Sons, Inc., New York, 1960).